Engineering Structures 195 (2019) 125–143

Contents lists available at ScienceDirect

Engineering Structures

journal homepage: www.elsevier.com/locate/engstruct

Effects of chord pre-load on strength of CHS X-joints stiffened with external ring stiffeners and gusset plates

Yong Chen[a], Zhongzheng Hu[a], Yong Guo[b], Jiyang Wang[a,*], Genshu Tong[a], Qingsong Liu[a], Yu Pan[b]

[a] College of Civil Engineering and Architecture, Zhejiang University, Hangzhou, China
[b] China Energy Engineering Group Zhejiang Electric Power Design Institute Co., Ltd., Hangzhou, China

ARTICLE INFO

Keywords:
Tubular joints
Stiffened X-joints
Finite element analysis
Chord stress function

ABSTRACT

Compared to unstiffened circular hollow section (CHS) X-joints, CHS X-joints stiffened with external ring stiffeners and gusset plates have exhibited much higher bearing capacity. To gain insight into the effects of the chord pre-loads on ultimate bearing capacity, this paper presents results of finite element (FE) analyses of the stiffened X-joints with braces under compression and chord under (i) axial load, (ii) in-plane bending moment, or (iii) combinations of axial load and in-plane bending moment. Precision of the FE model under combined brace and chord loads is validated by test results. The ultimate bearing capacities attained by using proportional loading and non-proportional loading respectively are presented, and the results indicate that the differences due to loading path are negligible. The validated FE modelling technologies are then employed in a parametric study on the effect of chord pre-load. A total of 4560 stiffened X-joints are examined in the parametric study. The theoretical analysis presented herein provides a reasonable explanation for the significant reduction in strength of stiffened X-joint when the chord is under axial tension. Finally, a chord stress function with corresponding boundary conditions is proposed, in which the coefficients for different chord load cases are determined through regression analysis. Furthermore, a lower-bound multiplier is given for the function to ensure a conservative design.

1. Introduction

It has been well recognized that chord load plays an important role in ultimate bearing capacity of tubular joints. Therefore, it is necessary to take into account the effect of chord load in the design of tubular joints. In companion paper [1], an innovative stiffened X-joint with external ring stiffeners and gusset plates is introduced, as shown in Fig. 1. This paper extends the investigation into the effects of chord loads on ultimate bearing capacity of stiffened X-joint.

To account for the effects of chord loading, chord stress/load function is usually adopted. The early study on the function can be traced back to the work by Togo [2], in which the effects of axial chord load on bearing capacity of X-joint were experimentally investigated. After that, Boone et al. [3] presented results of ten tests on identical large-scale double-tee (DT) specimens that were used to investigate the effect of uniform axial and bending chord stresses on strength of tubular joint. In addition, chord stress functions in terms of the combination of axial and bending stress were correspondingly proposed. Using the same chord nominal dimensions as in Boone's tests, Weinstein and Yura [4] completed thirteen tests to examine the effect of the ratio of brace diameter to chord diameter, β. It is found that for the DT-joints with $\beta = 1.0$, no reduction due to chord stress should be made for the specimens subjected to branch axial loading, whereas for the specimens with $\beta = 0.35$, there is a significant reduction in ultimate strength due to the chord load. By usage of the numerical simulation results based on the finite element (FE) models validated by Ha et al. [5], Pecknold et al. [6] proposed a parametric equation for the strength prediction of DT-joints with zero chord stress, and introduced a corresponding chord stress function that does not depend on chord thickness, but depends merely on β. Then, Pecknold et al. [7] extended their study to the case of that the chord is subjected to the combination of axial and bending pre-loads. Kang et al. [8] conducted three tests of X-joints subjected to both brace and chord compression loads to investigate the effect of chord stress. It is worth noting that both proportional loading and non-proportional loading were numerically studied. They concluded that the ultimate strength of DT-joint was unaffected by the load path used to apply combined loads. Then, they completed both numerical and experimental studies on the effects of chord axial compression on the

* Corresponding author.
E-mail address: kyotowang@zju.edu.cn (J. Wang).

https://doi.org/10.1016/j.engstruct.2019.05.076
Received 29 January 2019; Received in revised form 19 April 2019; Accepted 25 May 2019
Available online 06 June 2019
0141-0296/

Nomenclature

A	chord member cross-sectional area
A_{cc}	geometric parameter ($=(b_1 - T) + B_e T n_c$)
B_e	effective length of chord wall
C_1	coefficient (see Eq. (12), Tables 7 and 8)
C_2	coefficient (see Tables 7 and 8)
C_3	coefficient (see Tables 7 and 8)
C_4	coefficient (see Tables 7 and 8)
C_5	coefficient (see Table 7 and 8)
C_6	coefficient (see Table 9)
D	diameter of chord
E	Young's modulus
F	half of the resultant force transferred from the brace on ring plate
F_c	available stress
F_y	yield stress
H_g	height of gusset plate
L	length of chord
L_g	length of gusset plate
M_0	in-plane bending moment on chord
$M_{0,p}$	pre-bending moment on chord
M_a	required flexural strength (ASD)
M_c	nominal bending resultant in chord.
M_{bot}	reactive bending moment on section A (see Fig. 18)
M_{ipb}	nominal in-plane bending moment
M_{opb}	nominal out-of-plane bending moment
M_p	full-section plastic moment capacity
$M_{pl,0}$	full-section plastic moment capacity ($=[D^3 - (D - 2T)^3)]f_y/6$ for hollow circle section)
M_r	required flexural strength in hollow structural section
M_{top}	reactive bending moment on section B (see Fig. 18)
M_u	required flexural strength (LRFD)
N	compressive load on brace
N_0	axial load on the chord
$N_{0,p}$	axial pre-load on chord (positive values refer to tension)
$N_{pl,0}$	axial full-section yield capacity ($=\pi(D - T)T$ for hollow circle section)
P_a	required axial strength (ASD)
P_c	nominal axial load in chord.
P_r	required axial strength in hollow structural section
P_u	required axial strength (LRFD)
P_y	axial full-section yield capacity
Q_f	reduction factor or chord stress function
Q_{fd}	chord stress function for design
$Q_{f,FE}$	chord stress function obtained by FE analyses
Q_{fr}	reduction factor of resistance for ring plate ($=R/F$ ($n_0 = 0$))
$Q_{f,sug}$	suggested chord stress function (see Eq. (18))
$Q_{f,X}$	chord stress function for 'X' of which the subscript stands for 'CIDECT', 'AISC' or 'API'
R	resistance of ring plate ($=F(n_0)$)
R_T	radius of ring beam ($=D/2 - T + Y_c$)
S	chord elastic section modulus
T	thickness of chord wall
U	maximum chord stress (see Eq. (14))
Y_c	distance between centroid axis and innermost point of T-shape section
Y_r	distance between centroid axis and outmost point of T-shape section
a_1	height of tensile area in plasticity stage of T-shape section
b	coefficient (see Eq. (7))
b_1	height of compressive area in plasticity stage of T-shape section
c	coefficient (see Eq. (8))
d	diameter of brace
f_y	yield stress
f_u	ultimate tensile stress
h	height of T-shape section ($=T + w_r$)
l	length of brace
m_0	ratio of bending moment to plastic moment capacity of chord ($=M_{0,p}/M_{pl,0}$)
n	maximum chord stress (see Eq. (11))
n_0	ratio of axial pre-load to plastic capacity of chord ($=N_{0,p}/N_{pl,0}$), also ratio of normal stress in axial direction of chord to yield stress ($=\sigma_0/f_y$)
n_c	ratio of normal compressive stress in circumferential direction of chord to yield stress ($=\sigma_c/f_y$)
n_v	valid constant coefficient ($=0.8$)
t	thickness of brace wall
t_{br}	thickness of brace ring
t_g	thickness of gusset plate
t_r	thickness of chord ring
w_{br}	width of brace ring
w_r	width of chord ring
α	chord length to radius ratio ($=2L/D$)
α_g	moment ratio
β	brace to chord diameter ratio ($=d/D$)
γ	chord diameter to twice wall thickness ratio ($=D/(2T)$)
γ_d	lower-bound multiplier
γ_i	brace diameter to twice wall thickness ratio ($=d/(2t)$)
δ	relative displacement between the upper and lower brace rings (positive value indicates two brace rings approach to each other)
λ	gusset height to length ratio ($=H_g/L_g$)
σ_0	normal stress in axial direction of chord (positive values refer to tension)
σ_1, σ_2	principle stress
σ_c	normal compressive stress in circumferential direction of chord
τ	brace to chord wall thickness ratio ($=t/T$)
AISC	American institute of steel construction
API	American petroleum institute
ASD	allowable strength design
CHS	circular hollow section
CIDECT	Comité International pour Ie Développement et l'Étude de la Construction Tubulaire
COV	coefficient of variation
DT	double-tee
FE	finite element
LRFD	load and resistance factor design

ultimate strength of tubular DT-joint subjected to brace out-of-plane bending [9]. Van der Vegte and Makino [10] numerically investigated the effect of axial chord stress on strength of X-joint subjected to brace compression, and stated that for most X-joints, the tensile chord stresses lead to a reduction in ultimate strength. After that, van der Vegte et al. [11] made a reassessment on the effect of chord stress for the X-joints with brace compression, considering various chord loads: (i) axial load; (ii) in-plane bending moment; (iii) combinations of axial and in-plane bending moment, and new chord stress functions were concluded. Note that the recent studies extended the study on chord stress effects to thick-walled CHS X-joints [12,13]. These studies, as well as other relevant studies that are not included in this review, had strongly supported the design criteria of circular hollow section (CHS) X-joints with chord loading [14–16].

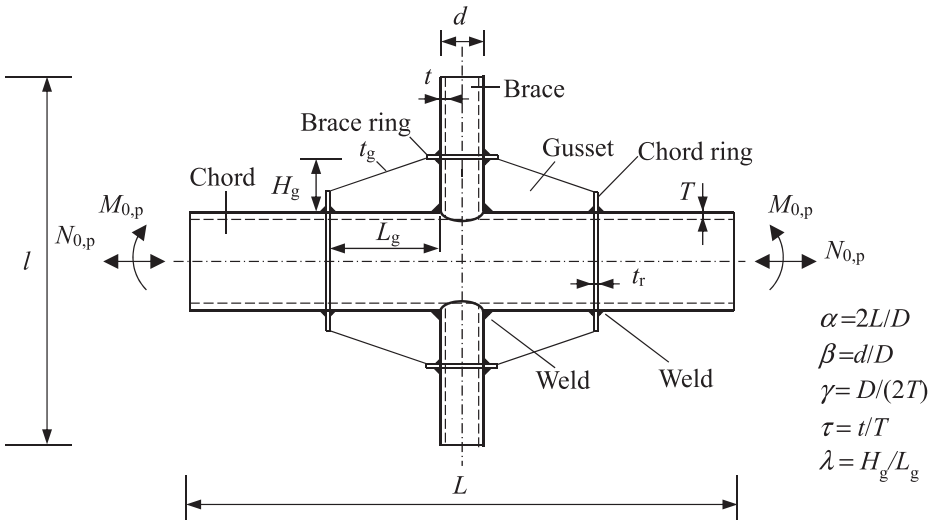

Fig. 1. Configuration and parameters of the stiffened X-joints.

However, the aforementioned studies are concerned with the effects of chord stress on strength of tubular X-joints with a traditional configuration. Obviously, without further study, it is not appropriate to employ these chord stress functions directly to consider the effect of chord load on strength of a stiffened X-joint. As shown in Fig. 1, this paper focuses on the performance of the newly developed stiffened X-joints [1] with braces under compression and chord under (i) axial load, (ii) in-plane bending moment, or (iii) combinations of axial load and in-plane bending moment. In Fig. 1, chord parameters incorporate diameter, D, thickness, T, and length, L. Brace parameters are diameter, d, thickness, t, and length, l. Gusset plate parameters are length, L_g, height, H_g, and thickness, t_g. Width and thickness of chord ring, and that of brace ring are denoted by w_r, t_r, w_{br} and t_{br} sequentially, where the subscript 'r' represents chord ring, and the subscript 'br' represents brace ring. Definition of non-dimensional parameters, α, β, γ, τ and λ are shown in Fig. 1.

In this paper, the FE models employed in the companion paper [1] have been slightly modified to facilitate imposing chord loads. The modified FE model is verified by comparing the calculated results with the experimental results. Parametric study is performed via the verified FE models to identify the predominate parameters that tend to have significant effects on the value of chord stress function. To explain the phenomenon of significant reduction in bearing capacity when the chord is under tension, a theoretical analysis is conducted. Finally, for design application, a chord stress function is proposed for the presented stiffened X-joint with chord under pre-load.

2. FE modeling

FE software ANSYS is employed in the numerical analyses. The FE modeling techniques have been discussed in the companion paper [1], and are briefly summarized as follows.

Shell element, namely SHELL 181 defined by ANSYS, is employed to simulate the entire structure as well as the welds. The placement and geometric dimensions of the welds are illustrated in Fig. 2. The weld around brace footprint is of $0.5t$ thick, whereas the fillet welds placed at the intersections of chord wall and rings are of $0.5t_r$ thick. A typical mesh is also shown in Fig. 2. With consideration of the stress concentration at the intersection of chord and brace, the mesh near the intersection is thus appropriately denser. The smallest element size is chosen to be of 3.5%D, according to the previous mesh convergence study [1].

In parametric study, the stress-strain curve is modelled by a perfect elastic-plastic relationship. Furthermore, the yield stress of the materials of chord, chord ring, gusset plates and welds around chord rings is 345 MPa, whereas the yield stress of the materials of braces, brace rings and welds at brace footprint is chosen to be 700 MPa to avoid premature failure of brace. In validation of FE modelling, true stress-strain relationship converted from engineering stress-strain relationship is adopted in the FE models of the experimental specimens, and the engineering stress-strain curves of chord, chord rings, braces, brace rings, and gusset plates are attained via material test.

Due to the symmetry of joint geometry and loading pattern, only one quarter or half of each joint was modelled, as shown in Fig. 2(a). For each node in the plane of symmetry, the translational displacement perpendicular to the plane of symmetry and two out-of-plane rotations are constrained. For the nodes at the ends of chord and braces, the nodal displacements in Z-direction are constrained. The axial loads applied to the tips of the braces are achieved by prescribing the vertical displacement of the nodes. Chord loads are directly applied at the connection point of rigid beams. Both geometric and material nonlinearities are considered in all the FE analyses in this study.

2.1. Modification of FE model

The FE model in the companion paper [1] is slightly modified herein in order to facilitate imposing loads on chords. As shown in Fig. 3, the end plates are replaced by rigid beams connecting the edge of the chord and the center point of the chord in radial fashion, and all of the beams are on the same plane. Thus, at the connection of the beams, the axial loading and bending moment can be applied.

2.2. Effect of loading sequence

Generally, in nonlinear analysis, different loading paths may result in different mechanical performances. Since both geometric and material nonlinearities are taken into account in the FE analyses of stiffened X-joints, it is necessary to analyze the effect of loading path. There are two loading paths: Path I, namely proportional loading, brace and chord loads increase gradually and proportionally, in which the load ratio is determined by non-proportional loading approach; Path II, namely non-proportional loading, chord load is firstly applied and maintained, and then brace load is applied by imposing displacements on the braces.

The load-displacement curves, as shown in Fig. 4, are attained by performing FE analyses of the stiffened X-joints with identical dimensions. The joints are subjected to five groups of chord pre-loads, which are imposed via two different load paths. The δ in the figure is the

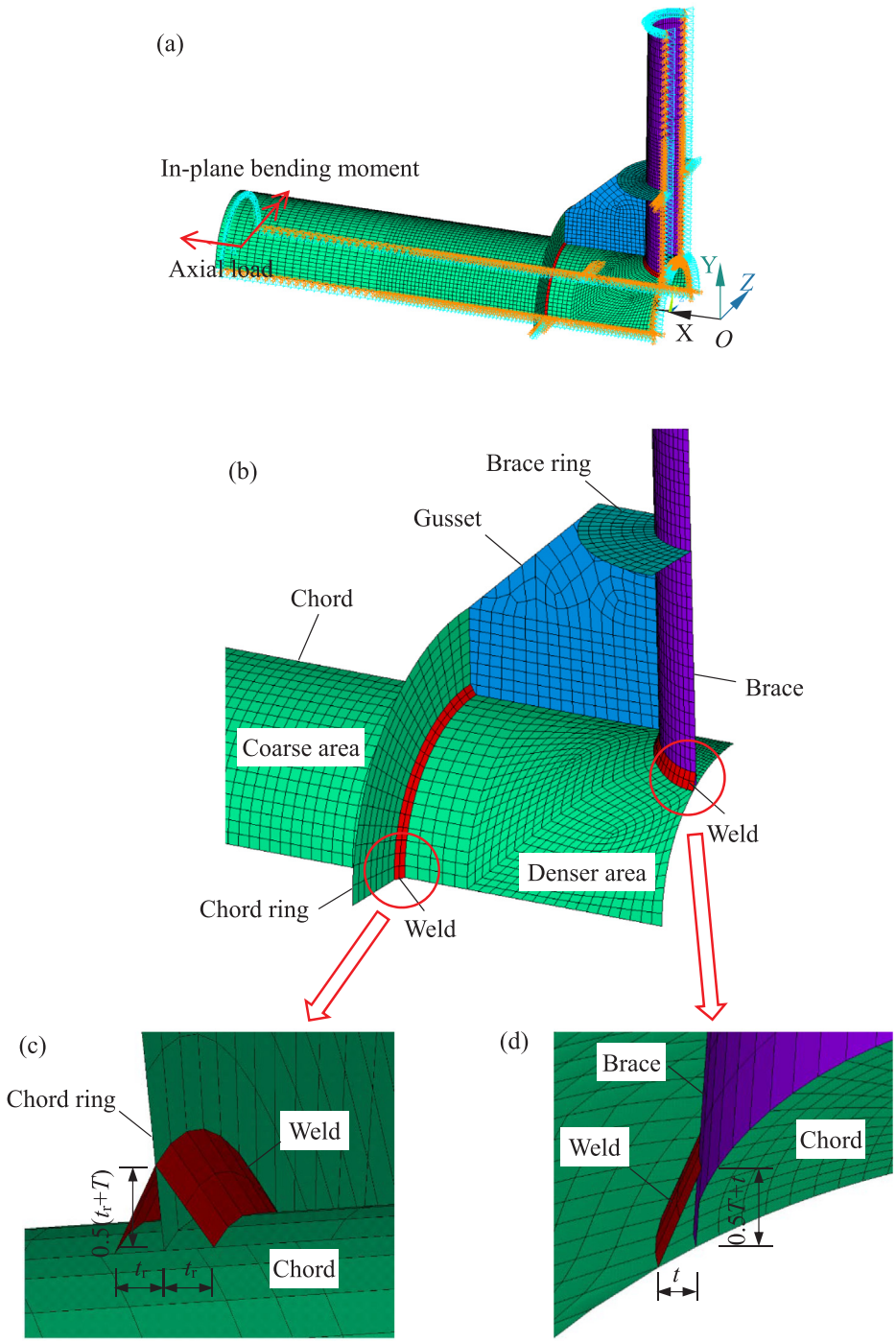

Fig. 2. FE model of one quarter of an X-joint. (a) Boundary condition and loads; (b) close-up of core area; (c) dimension of weld around chord ring; (d) dimension of weld around brace.

relative displacement between the upper and lower brace rings, and N is the axial load on the brace. It is found that the curves attained via two loading paths are close to each other, whether the chord pre-load is axial load, pure bending load, or combined loads. A slight inconsistency is found between the elastoplastic parts of the two curves, where the curve of the joint under proportional loading is a litter higher than that of the joint under non-proportional loading. However, within the deformation limit, this slight inconsistency can be reasonably disregarded. Thus, it can be concluded that the loading path has a negligible effect on ultimate bearing capacity of stiffened X-joint, which agrees well with the findings by Ha et al. [5], Kang et al. [8] and Choo et al. [12]. Accordingly, non-proportional loading, which is actually the load path adopted in the test, is chosen for the further numerical study for convenience.

2.3. Validation of FE model

Two nominally identical test specimens, numbered by XP1 and XP2, which are originally scaled down from a joint of Xihoumen long-span transmission tower located in Zhoushan, China, are set up for experimental study, in order to verify the FE modelling technologies. The geometrical dimensions of the specimens are listed in Table 1. Material tests were carried out to attain the material properties of each component of the joint. Material properties, namely the elastic modulus, E,

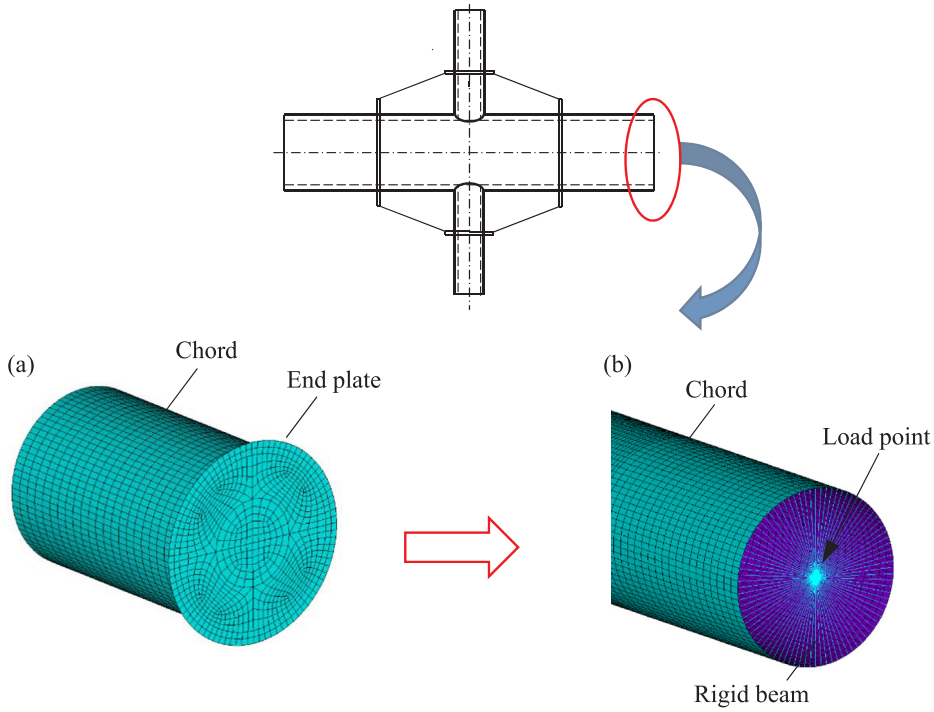

Fig. 3. FE models with (a) end plate, or (b) rigid beam.

yield strength f_y, and ultimate tensile strength f_u, are attained via the engineering stress-strain curve, and listed in Table 2.

Experimental setup is shown in Fig. 5, in which loading facility is a microchip controlled electro-hydraulic servo multifunction test machine being capable of producing uniaxial maximum compression load of 10,000 kN, and maximum tension load of 3000 kN. Four deformation transducers were employed to measure the deformation of the joint. The chord pre-loading system consists of a hydraulic jack, a reaction support and four tensile rods at chord end. According to the setup, the hydraulic jack exerts the axial force directly at one end of the chord, and the reaction from the jack supports is transmitted through the rods, being imposed on the other end of the chord. For convenience, non-proportional loading strategy was taken: through the hydraulic jack, compression loads are firstly imposed on the chord to 205 kN and maintained; after that, axial tension force is applied gradually to the tips of braces. To avoid the sudden rupture of the brace, which may cause damage to the field personnel, the maximum tensile loading applied to the brace tip in the test is less than 0.75 times of the ultimate tensile strength of the brace.

The load-displacement curves obtained from the test and the FE analysis are shown in Fig. 6. The results show that the specimens have entered the elastoplastic stage in the test. It is found that the experimental results are in good agreement with numerical results, especially the elastic part of the load-displacement curve. It can be concluded that the FE model established herein is capable of capturing the mechanic performance of the stiffened X-joints under chord pre-load.

3. Parametric study

3.1. Schemes of parametric analyses

In the companion paper [1], it is found that the strength of a stiffened X-joint mainly results from its chord and chord rings. Therefore, the main consideration in the parametric study is the effects of the geometric dimensions of chord and chord rings. Besides, as the gusset plates that transfer partial axial loadings of the braces to the chord rings may have an effect on load-transferring path and further affect the ultimate bearing capacity of stiffened X-joint, the effect of the dimensions of the gusset plates is therefore considered. Based on these considerations, three calculation schemes are set up and listed in Tables 3–5. In detail, Scheme 1 shown in Table 3 is for surveying the effects of the dimensions of chord and gusset plates on chord stress function, Scheme 2 shown in Table 4 is for surveying the effects of the dimensions of chord rings and gusset plates, and Scheme 3 shown in Table 5 is for surveying the effects of the dimensions of chord, chord rings and gusset plates. FE-based parametric analyses are performed for a wide range of geometrical parameters, i.e. $10 \leqslant \gamma \leqslant 50$, $\beta \leqslant 0.9$, $0.43 \leqslant \lambda \leqslant 1.0$, $w_r/t_r \leqslant 20$, $0.4 \leqslant t_r/T \leqslant 2.5$.

As shown in Fig. 1, three chord pre-load cases are considered to be imposed on the chord of each joint individually: (i) axial load; (ii) in-plane bending moment; (iii) combination of axial load and in-plane bending moment. Details of chord pre-loads are summarized in Table 6. Non-proportional loading strategy is taken, which means that the chord load is imposed prior to the brace loadings. Details of three chord pre-load cases are as follows.

1) Axial load. Chord pre-load ratio $n_0 = N_{0,p}/N_{pl,0}$, is utilized to define the axial loading level, in which $N_{0,p}$ is axial load, and $N_{pl,0} = \pi(D\text{-}T)T$ is plastic axial capacity of cross section of chord. Each stiffened X-joint, listed in Tables 3–5, is analyzed for $n_0 = -0.9, -0.8, -0.6, -0.3, +0.3, +0.6, +0.8$, and $+0.9$, where the negative values refer to compression, and positive values refer to tension.
2) In-plane bending moment. Each stiffened X-joint listed in Tables 3–5 is analyzed for pre-bending moment ratios $m_0 = M_{0,p}/M_{pl,0} = -0.9, -0.8, -0.6, -0.3$. $M_{0,p}$ is pre-bending moment imposed on the chord, and $M_{pl,0} = [D^3 - (D - 2T)^3]f_y/6$ [17] is the plastic bending moment capacity of chord cross section. The direction of the bending moment is shown in Fig. 1. Because the compressive side will govern the strength of these joints, the bending moments are taken as negative [11].
3) Combination of axial load and in-plane bending moment. According to the preliminary studies of the joints with pure axial pre-loads or pure pre-bending moments, it is found that geometric parameters β, λ and w_r have more effects on the chord stress function, while the effects of other geometric parameters are relatively less. In the light of the above fact, only the stiffened X-joints with dimensions listed

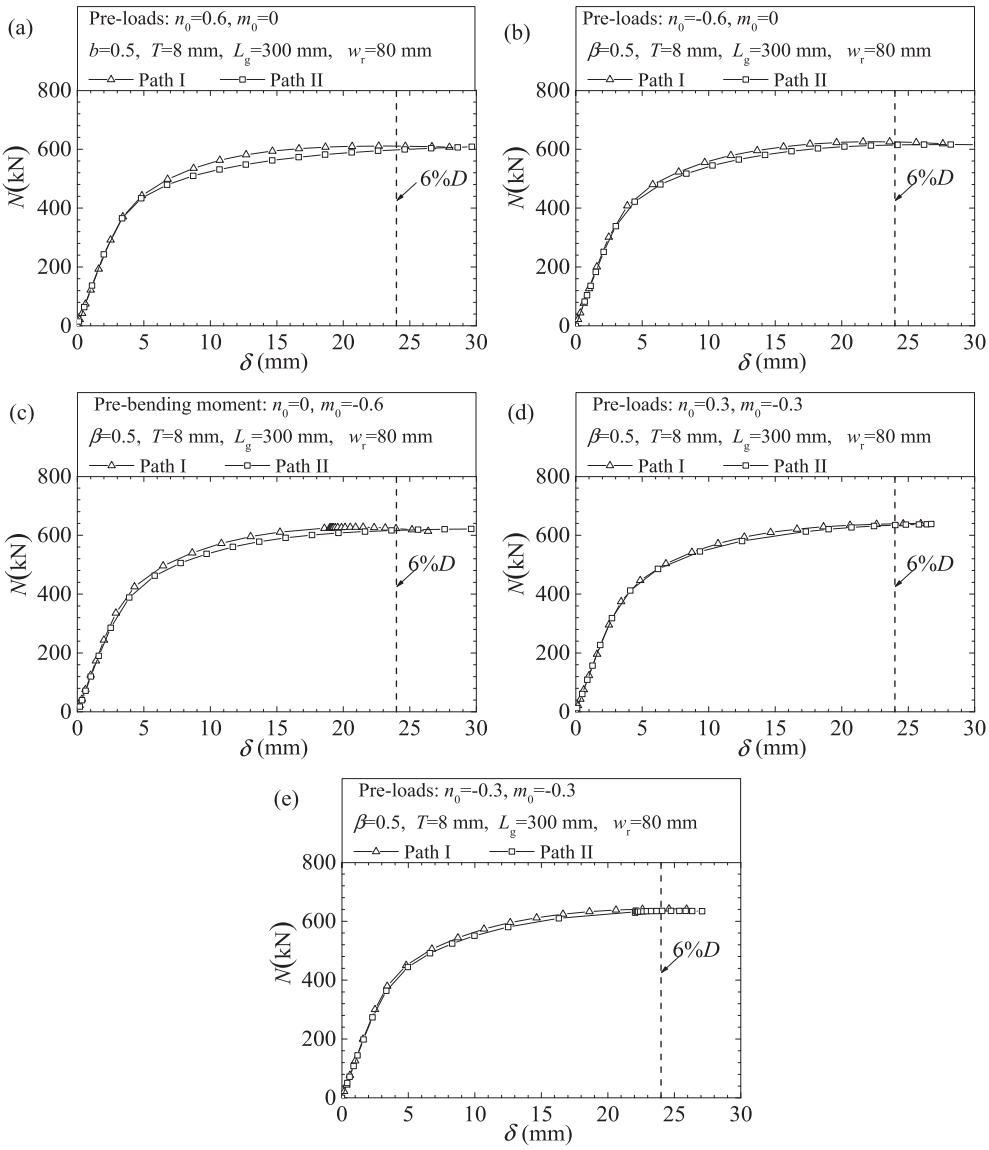

Fig. 4. Load-displacement for X-joints under different load paths and chord loads. Chord loads: (a) axial tension; (b) axial compression; (c) in-plane bending moment; (d) combination of axial tension and in-plane bending moments; (e) combination of axial compression and in-plane bending moments. Path I: proportional loading; Path II: non-proportional loading.

in Table 3 are surveyed. In addition, each joint is pre-loaded with eighteen combinations of n_0 and m_0, listed at the right two columns of Table 6.

3.2. Effects of chord pre-loads

Fig. 7 shows von Mises stress distributions and deformations of six X-joints subjected to chord loads, at deformation limit i.e. 6%D. These joints have identical dimensions, namely $\beta = 0.7$, $\gamma = 25$, $L_g = 500$ mm, $w_r = 160$ mm, $t_r = 8$ mm. Chord pre-loads for these six joints are combinations of $(m_0,n_0) = (0,0.6)$, $(0,-0.6)$, $(-0.6,0)$, $(0.3,-0.3)$, $(-0.3,-0.3)$, $(0,0)$, sequentially. It is observed that in all these joints, large deformations commonly appear at the intersection of chord and brace. Moreover, the yielded areas are majorly observed in three parts: (1) the chord wall between two chord rings, (2) the chord wall near chord rings, and (3) chord rings. Compared to the stiffened X-joints without pre-load on chord, the stiffened X-joints with chord pre-load can be found with much more yielded areas. It is noted that to

Table 1
Geometric dimensions of specimens [a].

Specimen	Chord			Brace			Gusset plate			Chord ring		Brace ring	
	D(mm)	T(mm)	L(mm)	d(mm)	t(mm)	l(mm)	L_g(mm)	H_g(mm)	t_g(mm)	w_r(mm)	t_r(mm)	w_{br}(mm)	t_{br}(mm)
XP1	403	7.8	2500*	124	4.3	2200*	170*	100*	10.2	66	7.9	32	13.1
XP2	403	7.9	2500*	124	4.2	2200*	170*	100*	10.7	66	7.8	33	13.2
Mean	403	7.8	2500*	124	4.2	2200*	170*	100*	10.4	66	7.8	32	13.6

[a] Except for the nominal values marked with asterisks, the others are measured values.

Table 2
Material properties of major joint components.

Component	E(MPa)	f_y(MPa)	f_u(MPa)
Chord	2.07×10^5	394	538
Brace	2.07×10^5	462	589
Chord ring	2.06×10^5	398	544
Brace ring	2.09×10^5	370	489
Gusset plate	2.10×10^5	383	550

highlight the stress distribution of the chord, the von Mises stress contours are illustrated with the stress below maximum yield stress of chord.

Fig. 8 shows the load-displacement curves of the six X-joints illustrated in Fig. 7. A slight enhancement is found in the curves of the joints with compressive chord forces, whereas a notable reduction in strength is observed in the joints subjected to tensile chord forces. This finding appears to present a phenomenon differing from previous work [11] which demonstrated an enhancement effect of tensile pre-loads on unstiffened X-joints. It is therefore necessary to further study the mechanism of stiffened X-joints subjected to pre-loads, which will be explored carefully in Section 4.

Part of numerical results is illustrated in Figs. 10–17. In the figures, Q_f is the chord stress function, i.e. ratio of strength of the joint with chord pre-load to that of the same joint without chord pre-load. The analyses for stiffened X-joints under three chord pre-load cases are stated as follows.

1) Axial load. It can be observed from Figs. 10–12 that the axial compression and the axial tension have obviously different impacts on ultimate bearing capacity. In general speaking, the effect of the pre-compression is rather small, but the effect of pre-tension is significant. It is found that in case of moderate pre-compression, there is a slight enhancement of the strength, whereas a reduction in strength is observed in case of large pre-compression. Furthermore,

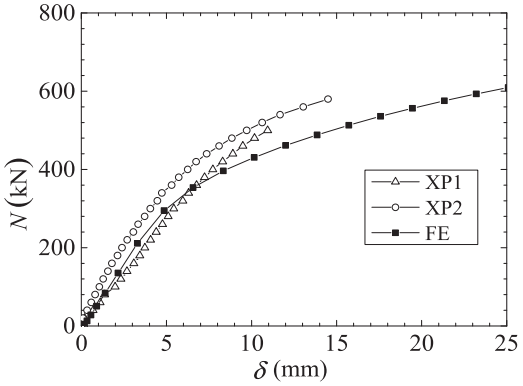

Fig. 6. Load-displacement curves obtained by tests and numerical analyses.

Table 3
Summary of geometric parameters for Scheme 1*.

$D \times T$ (mm × mm)	β	λ	w_r (mm)
400 × 8	0.30, 0.50, 0.70, 0.90	0.43, 0.50, 0.60, 0.75, 1.00	80, 120, 160, 200

* $L = 3200$ mm, $l = 2200$ mm, $t = 8$ mm, $H_g = 300$ mm, $t_g = 20$ mm, $t_r = 8$ mm, w_{br}=max(80 mm, d/2), $t_{br} = 16$ mm.

Table 4
Summary of geometric parameters for Scheme 2**.

$D \times T$ (mm × mm)	λ	w_r (mm)	t_r (mm)
400 × 8	0.43, 0.50, 0.60, 0.75, 1.00	80, 120, 160, 200	8, 12, 16, 20

** $L = 3200$ mm, $l = 2200$ mm, $d = 200$ mm, $t = 8$ mm, $H_g = 300$ mm, $t_g = 20$ mm, w_{br}=max(80 mm, d/2), $t_{br} = 16$ mm.

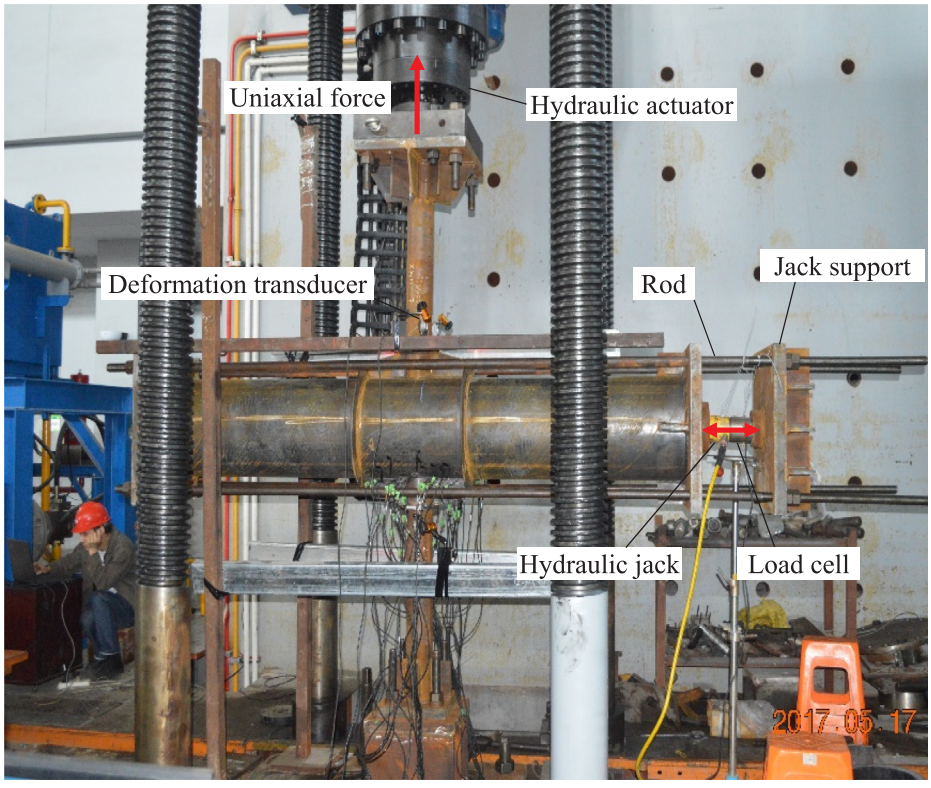

Fig. 5. Experimental setup.

Table 5
Summary of geometric parameters for Scheme 3[***].

$D \times T$ (mm)	γ	β	λ
400 × 8	10.0, 16.7, 25.0, 50.0	0.30, 0.50, 0.70, 0.90	0.43, 0.50, 0.60, 0.75, 1.00

*** $L = 3200$ mm, $l = 2200$ mm, $t = 8$ mm, $H_g = 300$ mm, $t_g = 20$ mm, $w_r = 120$ mm, $t_r = 8$ mm, w_{br}=max(80 mm, $d/2$), $t_{br} = 16$ mm.

if the chord is under tension, significant decrease in chord stress function is found as the tension force increases. Summarily, the chord stress effect is more sensitive to the geometric dimensions of chord, chord rings and gusset plates in case of pre-tension than that in case of pre-compression. Among the geometric parameters utilized for analysis, it is found that β, λ and w_r have much greater effects on ultimate bearing capacity.

The above findings may be explained as follows. According to Chen's work [1], the bearing capacity of stiffened X-joint consists predominantly of two parts. One of them, defined as Part I, originates from the resistance of chord wall at the intersection of chord and brace, and the other one, defined as Part II, originates from the resistance of the ring beam being composed of the chord ring plate and the chord wall with an effective width. Fig. 9 shows the von Mises stress distribution of the stiffened X-joints subjected merely to axial pre-loads. As can be seen from Fig. 9, due to the existence of gusset plates, chord pre-load is transmitted from the chord to the brace, which consequently reduces the stress level of the area between two chord rings. Therefore, the effect of chord stress on Part I of stiffened X-joints is less than that of unstiffened X-joints. In addition, Part II usually accounts for half or more of the total bearing capacity of stiffened joints. Thus, the effect of chord stress on Part II is more remarkable. That is to say, the curve of chord stress function of stiffened X-joint is between the curves of Part I and Part II, but closer to the curve of Part II. A significant reduction of Part II caused by tensile chord stress will result in a corresponding remarkable reduction in ultimate bearing capacity of stiffened X-joint, since Part II predominates. For Part II affected by axial chord pre-loads, a detailed theoretical analysis will be given in Section 4. It is concluded in Section 4 that Part II is more sensitive when the chord is under tension, which approves the findings from Figs. 10–12.

2) In-plane bending moment. In Figs. 13–15, the chord stress functions of the stiffened X-joints subjected to in-plane bending moment show negligible dependence on geometric parameters, which is similar to that of the joints under axial compressive pre-loads. In addition, the chord stress function in this case appears to be between that of a joint with chord under axial pre-compression and that of a joint with chord under axial pre-tension, which may be related to the fact that the cross section of chord is under partially compressive and partially tensile stresses. In Fig. 15, the data of the joint with $T = 4$ mm and $m_0 = -0.9$ are eliminated because premature bulking occurs in chord due to its excessively thin wall and large stress. From Fig. 13(b), it is observed that the Q_f with a large α_g is a little irregular, where α_g is the ratio of moments, namely the moment of reaction of chord ring about crown point to the moment of reaction of brace ring about the same crown point [1]. According to Chen's work [1], if $\alpha_g > 0.8$, the bearing capacity of stiffened X-joint becomes uncertain and unstable, for which the case should be avoided.
3) Combination of axial force and in-plane bending moment. For the stiffened X-joints subjected to combinations of chord axial load and in-plane bending moment, the performance is similar to the joints subjected to axial chord pre-load or that subjected to in-plane bending moment merely. It depends on which one is dominant. Fig. 16 illustrates the data of the joints subjected to combinations of $|n_0| = 0.3$ and m_0. It is observed that the joint under combination of $n_0 = -0.3$ and a specified m_0 has a slightly higher bearing capacity than the joint under combination of $n_0 = 0.3$ and an identical bending moment. Generally, chord stress function of a joint with a low chord axial load namely $|n_0| = 0.3$ is not sensitive to geometric parameters. However, in Fig. 17 for the joints with a low chord bending moment namely $|m_0| = 0.3$, the chord stress function is more sensitive to the geometric parameters, especially in the case of chord pre-tension. In addition, it is worth noting that in case of $|m_0| = 0.3$, the enhancing effect of chord pre-compression on bearing capacity is unapparent. Moreover, the adverse effect of chord pre-tension becomes attenuate relatively. This may be attributed to the counteracting effect of the bending moment on the chord axial pre-load.

Table 7
Summary of values for coefficients C_1, C_2, C_3 [*].

	C_1	C_2	C_3
$\beta \leqslant 0.9$	0.2	0	0.5
$\beta = 1.0$	−0.2	0	0.2

* Linearly interpolated values between $\beta = 0.9$ and $\beta = 1.0$ for X joints under brace axial loading.

4. Theoretical analysis

It is found that there exist apparent differences between stiffened and unstiffened X-joints under chord pre-load. In comparison of unstiffened joints, stiffened X-joints possess two chord ring plates providing extra strength. The existence of external ring plates is exactly the reason that the stiffened X-joints exhibit distinct performance. The following theoretical analysis attempts to explain the impacts originating from the ring plates.

According to the work by Lee et al. [18], a ring beam that is comprised of a chord wall with an effective flange width, i.e. B_e, and a chord ring is employed to establish a simplified mechanical model, as shown in the left picture of Fig. 18(a). Taking advantage of the symmetry of the model, a quarter of the ring beam is used with guide supports on its two ends, as shown in the right of Fig. 18(a). Based on elastic theory, the cross section A-A is subjected to a combination of compression and bending moment. The bending moment M_{bot}, can be given by

Table 6
Summary of loads on chords.

Axial load $n_0 = N_{0,p}/N_{pl,0}$	In-plane bending moment $m_0 = M_{0,p}/M_{pl,0}$	Combinations of axial load and in-plane bending moment		
		Axial load $n_0 = N_{0,p}/N_{pl,0}$		In-plane bending moment $m_0 = M_{0,p}/M_{pl,0}$
−0.9, −0.8, −0.6, −0.3, 0.3, 0.6, 0.8, 0.9	−0.9, −0.8, −0.6, −0.3	−0.7		−0.1, −0.2, −0.3
		−0.5		−0.2, −0.3, −0.5
		−0.3	+	−0.3, −0.5, −0.7
		0.3		−0.3, −0.5, −0.7
		0.5		−0.2, −0.3, −0.5
		0.7		−0.1, −0.2, −0.3

Table 8
Values for coefficients in Eq. (18).

Chord force	C_1	C_2	C_3	C_4	C_5	No. of data	Mean	COV
Axial compression	0.40	0.60	−1.0	0.37	0.15	405	1.00	2.5%
Axial tension	0.52	−1.9	2.8	1.4	0.07	405	0.99	5.4%
Bending	−0.40	−0.07	−0.20	0.93	0.11	405	1.00	1.8%
Axial compression + bending	−0.94	0.50	−1.0	0.95	0.28	424	1.01	2.2%
Axial tension + bending	−0.01	−0.24	0.47	0.26	−0.08	424	0.99	6.5%

$$M_{bot} = FR_T\cdot\left(1-\frac{2}{\pi}\right) \tag{1}$$

where F is half of the resultant force from the brace. R_T is the radius of the ring beam, i.e. $R_T = D/2 - T + Y_c$. Y_t and Y_c are the distances between centroid axis and outmost and innermost points of T-shape section, respectively.

According to Chen's work [1], the bearing capacity of the chord ring is determined by the resistance of cross section A-A. Assuming that part of cross section A-A enters elastoplastic stage, the section will possess a stress distribution shown in Fig. 18(d). Since the chord element of section A-A is in a two-dimensional stress state shown in Fig. 18(b), the chord element yields with a normal stress of $n_c f_y$. Von Mises yield criterion for in-plane stress state yields

$$f_y = \sqrt{\sigma_1^2 - \sigma_1\sigma_2 + \sigma_2^2} \tag{2}$$

Let $\sigma_1 = \sigma_0$, $\sigma_2 = -\sigma_c$, $n_0 = \sigma_0/f_y$, $n_c = \sigma_c/f_y$, Eq. (2) yields

$$n_c = \sqrt{1 - 0.75n_0^2} - 0.5n_0 \tag{3}$$

where σ_1 and σ_2 are principle stress, σ_0 is normal stress in axial direction of chord, σ_c is the normal compressive stress in circumferential direction of chord. Note that positive value of σ_c means compression.

Balance of forces on cross section A-A leads to

$$F - (A_{cc} - t_r a_1)f_y = 0 \tag{4}$$

$$FY_c - M_{bot} + t_r a_1\left(h - \frac{a_1}{2}\right)f_y + \frac{1}{6}t_r(h - a_1 - b_1)^2 f_y - \frac{1}{2}t_r (b_1^2 - T^2)f_y - \frac{1}{2}B_e T^2 n_c f_y = 0 \tag{5}$$

where $A_{cc} = (b_1 - T) + B_e T n_c$, $h = T + w_r$, a_1 and b_1, as shown in Fig. 18(d), are the heights of the tensile and compressive areas in plastic stage respectively. Then, the solution of F, as a function of n_0, is

$$F(n_0) = \frac{-b + \sqrt{b^2 - 4c}}{2} f_y \tag{6}$$

where

$$b = t_r\left[3\left(1-\frac{2}{\pi}\right)R_T - 3Y_t + 2h + b_1\right] - 2A_{cc} \tag{7}$$

$$c = \frac{1}{2}t_r^2(2b_1^2 + 2hb_1 - h^2 - 3T^2) + \frac{3}{2}t_r B_e T^2 n_c - t_r A_{cc}(2h + b_1) + A_{cc}^2 \tag{8}$$

According to the plastic development coefficient proposed by Chen et al. [1], it is found that b_1 is around $0.2h$. By assuming a constant $b_1 = 0.2h$ in Eq. (5), one may obtain the resistance of the ring $R = F(n_0)$, dependent on n_0.

For example, defining a reduction factor of resistance of ring plates, that is

$$Q_{fr} = R/F(n_0 = 0) \tag{9}$$

and taking the joints of $D = 400$ mm, $\beta = 0.5$, $\gamma = 25$, along with various w_r or t_r, curves of Q_{fr} that is varying with n_0 are illustrated in Fig. 19. It is observed that if n_0 is positive, Q_{fr} decreases significantly with increase of n_0, and Q_{fr} is less than 1.0. Nevertheless, if n_0 is negative, Q_{fr} is always greater than 1.0, and a peak appears in the vicinity of $n_0 = -0.6$. Obviously, Q_{fr} shows distinct performance, in comparison of the chord stress function of unstiffened X-joints. However, as analyzed in Section 3.2, the chord stress function of stiffened X-joint exhibits remarkable similarity to Q_{fr}, because the resistance of the chord ring predominates in the overall bearing capacity of the whole joint.

5. Chord stress function

5.1. Reported chord stress functions

Many studies on chord stress function for unstiffened X-joints have been reported and referenced in various specifications, design standards and codes. The formulae used in various codes are listed below, mainly in two forms, namely exponential and quadratic forms.

5.1.1. Cidect (2008)/IIW (2012)/ISO (2013)

Chord stress function recommended by Comité International pour Ie Développement et l'Étude de la Construction Tubulaire (CIDECT) [19], International Institute of Welding (IIW) [20], and International Organization for Standardization (ISO) [21] has an exponential form of

$$Q_f = (1 - |n|)^{C_1} \tag{10}$$

with

$$C_1 = \begin{cases} 0.45 - 0.25\beta, & \text{if } n < 0 \\ 0.20, & \text{if } n \geqslant 0 \end{cases} \tag{11}$$

and

$$n = \frac{N_0}{N_{pl,0}} + \frac{M_0}{M_{pl,0}} \tag{12}$$

in connecting face. N_0 and M_0 are the axial load and in-plane bending moment on the chord. $N_{pl,0}$ is the axial full-section yield capacity and $M_{pl,0}$ is the full-section plastic moment capacity. It should be noted that the most punitive stress effect of Q_f in the chord on either side of the joint is to be used.

5.1.2. AISC (2010)

If the chord is under compression, the form of reduction factor recommended by American Institute of Steel Construction (AISC) [22] is

$$Q_f = 1.0 - 0.3U(1 + U) \tag{13}$$

where

Table 9
Values for coefficient of lower -bound multiplier.

Coefficient	Axial compression	Axial tension	Bending	Axial compression + bending	Axial tension + bending
C_6	0.2	0.4	0.2	0.2	0.4

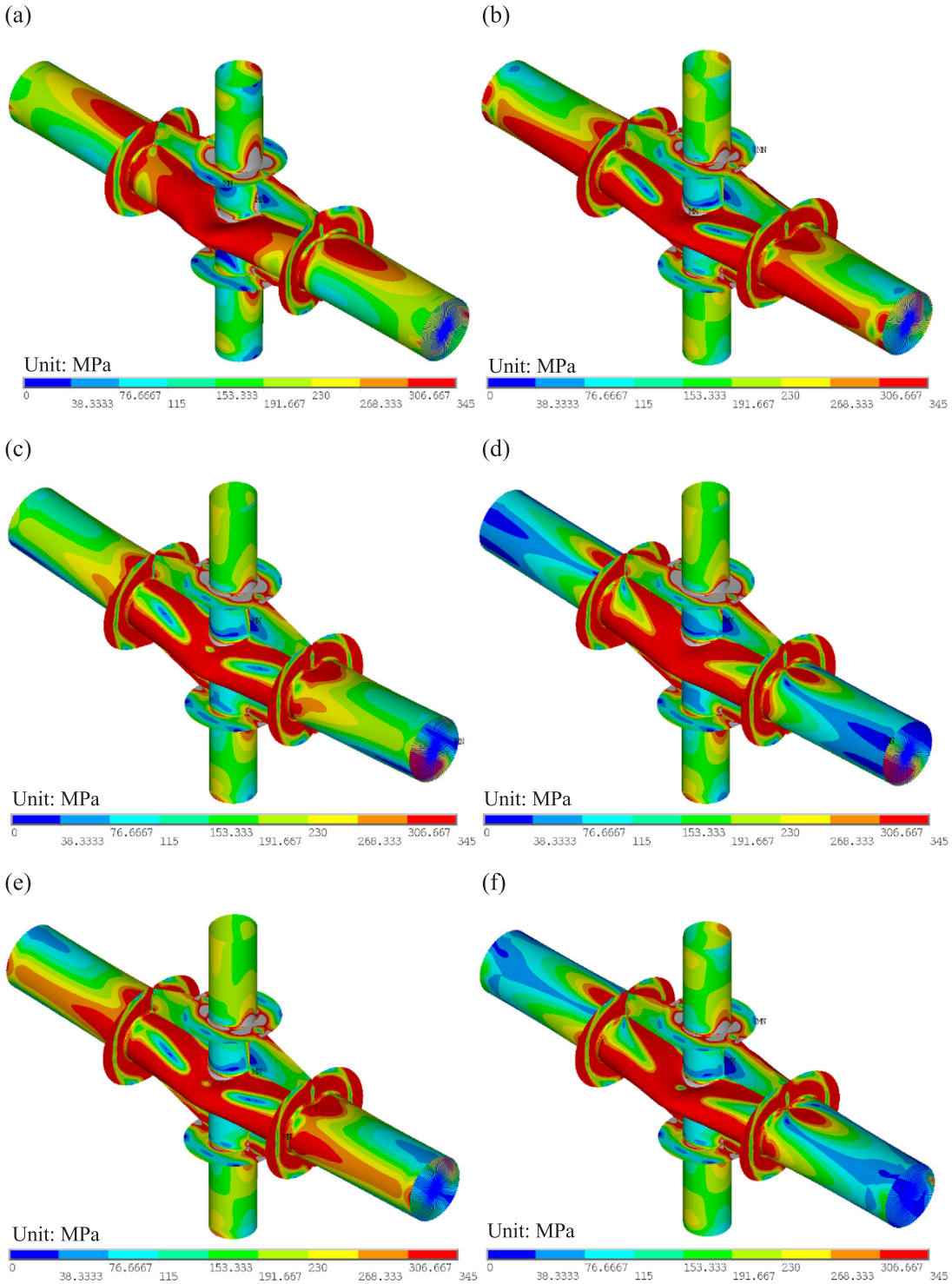

Fig. 7. Von Mises stress distributions of X-joints with chords subjected to (a) axial tension; (b) axial compression; (c) in-plane bending moments; (d) combinations of axial tension and in-plane bending moments; (e) combinations of axial compression and in-plane bending moments; (f) no chord pre-load.

$$U = \left| \frac{P_r}{AF_c} + \frac{M_r}{SF_c} \right| \tag{14}$$

If the chord is under tension, effect of chord stress is ignored, i.e. $Q_f = 1.0.P_r$ and M_r are determined on the side of the joint that has the lower compression stress, referring to required axial and flexural strength in hollow structural section respectively. $P_r = P_u$ in load and resistance factor design (LRFD); $P_r = P_a$ in allowable strength design (ASD). $M_r = M_u$ in LRFD; $M_r = M_a$ in ASD. P_a and M_a are required axial and flexural strength respectively for ASD. P_u and M_u are required axial and flexural strength respectively for LRFD. F_c = available stress = F_y (LRFD) or 0.6 F_y (ASD). A = chord member cross-sectional area. S = chord elastic section modulus.

5.1.3. API (2014)xx

Chord stress function recommended by American Petroleum Institute (API) [23] is in a form of

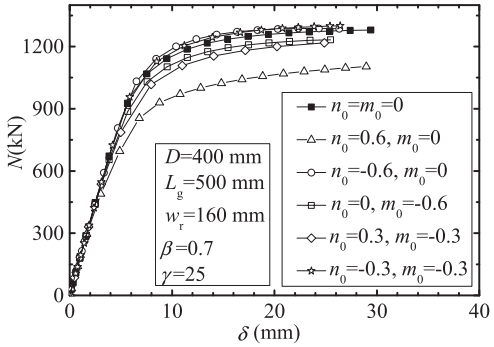

Fig. 8. Load-displacement curves for stiffened X-joints with different chord pre-loads.

$$Q_f = \left[1 + C_1\left(\frac{P_c}{P_y}\right) - C_2\left(\frac{M_{ipb}}{M_p}\right) - C_3 A^2\right] \tag{15}$$

where

$$A = \left[\left(\frac{P_c}{P_y}\right)^2 + \left(\frac{M_c}{M_p}\right)^2\right]^{0.5} \tag{16}$$

$$M_c^2 = M_{ipb}^2 + M_{opb}^2 \tag{17}$$

and values of C_1, C_2, C_3 are listed in Table 7.

P_c and M_c are the nominal axial load and bending resultant in the chord respectively. M_{ipb} and M_{opb} are nominal in-plane and out-of-plane bending moments respectively. P_y is the yield axial capacity of the chord, M_p is the plastic moment capacity of the chord, and C_1, C_2 and C_3 are coefficients depending on joint configuration and load type. The average of the chord loads as well as bending moments on either side of the brace intersection should be used in Eq. (15). Chord axial load is positive if it is tension force, the chord in-plane bending moment is positive when it produces compression on the joint footprint.

5.2. Chord stress function for stiffened X-joints

It is found that the variation of Q_f with chord pre-load is similar to that of n_c with n_0. Taking the form of n_c, and considering the effect of geometric parameters which are chosen as exponent, the chord stress function is considered to be in a form of

$$Q_f = (\sqrt{1 - 0.75n^2} + C_5 n)^{C_1\beta + C_2\lambda + C_3 w_r/D + C_4} \tag{18}$$

where

$$n = |n_0| + |m_0| \tag{19}$$

This form has $Q_f = 1.0$ for $n = 0$ and can also reflect the characteristics of the enhancement found in some joints in which the chord is under pre-compression. Geometric parameters, namely β, λ and w_r, are chosen as independent variables, because these parameters have a greater effect on chord stress function than others.

The values of coefficients in Eq. (18), namely C_1, …, C_5, are determined via regression analysis, and listed in Table 8. It is found that the dispersion gets much smaller if axial compression is in presence. For compressive pre-loads cases, the minimum value of the coefficient of variation (COV) is 1.8. Fig. 20 shows the dispersion of $Q_{f,FE}/Q_{f,sug}$, where $Q_{f,FE}$ is the chord stress function obtained by FE analyses and $Q_{f,sug}$ is the chord stress function obtained via Eq. (18). In the figure, sgn (·) is the sign function.

To ensure a conservative design, a chord stress function, Q_{fd}, is employed to take place of Q_f, the relationship between them is

$$Q_{fd} = \gamma_d Q_f \tag{20}$$

where γ_d is termed lower-bound multiplier, and in a form of

$$\gamma_d = 1 - C_6 n^2 \tag{21}$$

In Eq. (21), the values of C_6 for different chord pre-loads are listed in Table 9.

The valid ranges of geometric parameters are $10 \leqslant \gamma \leqslant 50$, $\gamma_i \leqslant 30$, $\beta \leqslant 0.9$, $w_r/t_r \leqslant 20$, and $\alpha_g \leqslant 0.8$ [1]. The valid ranges of load ratios are $|n_0| \leqslant n_v$ for axial pre-load, $|m_0| \leqslant n_v$ for pre-bending moment and $|n_0|^{1.7} + |m_0| \leqslant n_v$ [24] for combination of axial load and bending moment, where n_v is the valid constant coefficient, that is $n_v = 0.8$. It is worth noting that a large n tends to result in remarkable difference between results obtained by proposed formulation and numerical results.

5.3. Comparison between the proposed and reported equations

For an intuitive comparison of the reported formulas in Section 5.1 for unstiffened X-joints and the proposed chord stress function in Section 5.2 for stiffened X-joints, the results achieved by the formulae and FE analysis are illustrated in Fig. 21. A stiffened X-joint that has typical geometric dimensions of $\beta = 0.5$, $\gamma = 25$, $\lambda = 1.0$, $w_r/D = 0.3$ and $t_r/T = 1.0$ is employed. It can be identified that the results via FE analyses have a good agreement with the results obtained by Eq. (18).

It is found that the results obtained by the proposed formulation herein are generally greater than the results obtained by the formulations recommended in specifications, in case of chord compression load. When chord tension load is involved, the results of Q_{fd} attained via Eq.

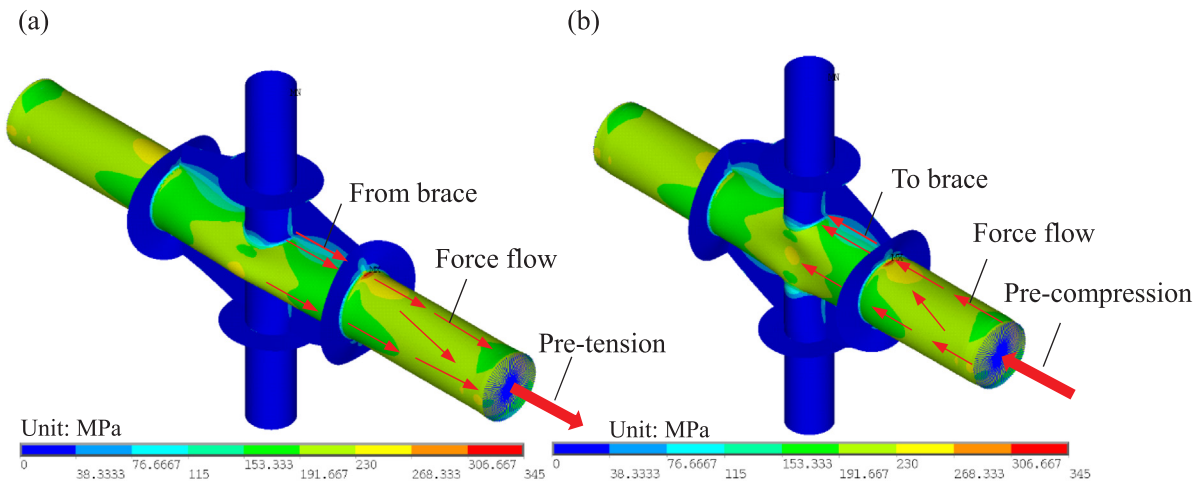

Fig. 9. Von Mises stress distribution for joints under (a) pre-tension; or (b) pre-compression.

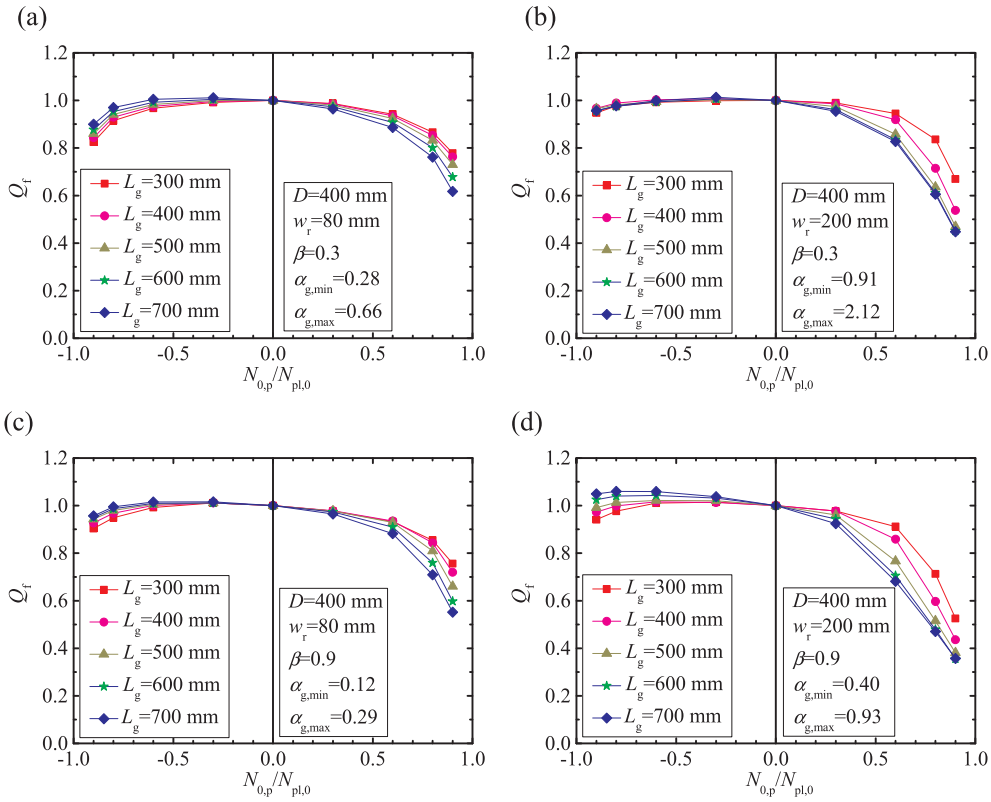

Fig. 10. Chord stress function for joints under axial loads (Scheme 1). (a) β = 0.3, w_r = 80 mm; (b) β = 0.3, w_r = 200 mm; (c) β = 0.9, w_r = 80 mm; (d) β = 0.9, w_r = 200 mm.

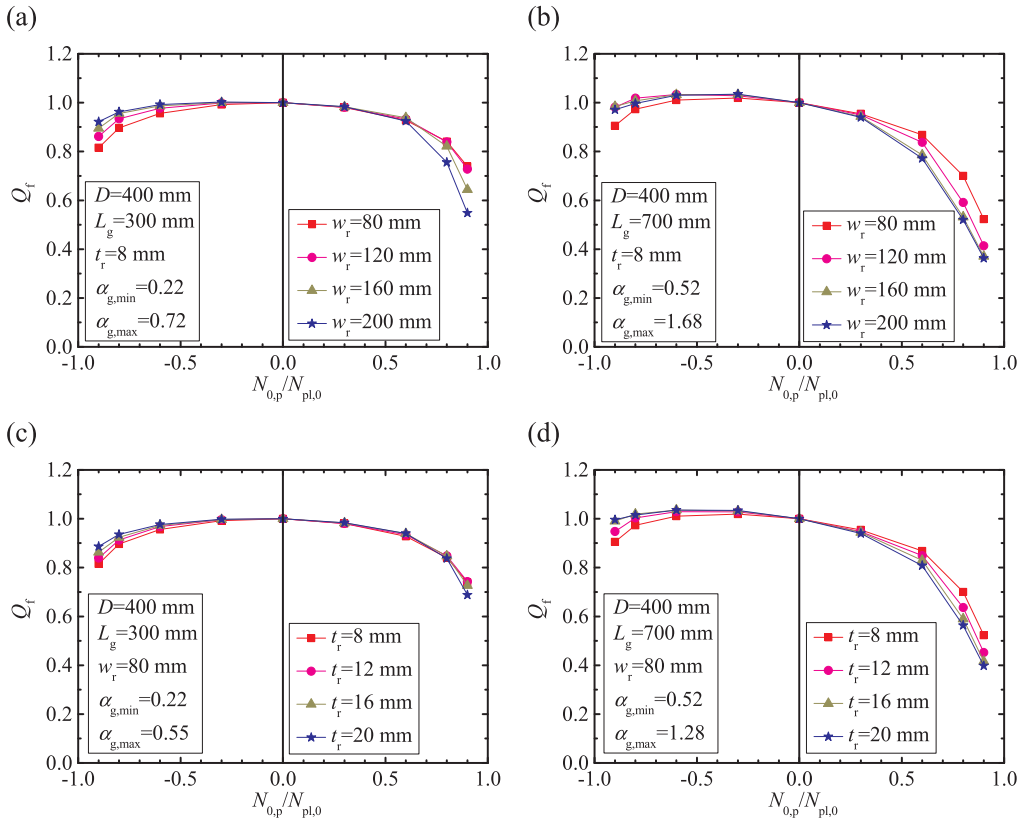

Fig. 11. Chord stress function for joints under axial loads (Scheme 2). (a) L_g = 300 mm, t_r = 8 mm; (b) L_g = 700 mm, t_r = 8 mm; (c) L_g = 300 mm, w_r = 80 mm; (d) L_g = 700 mm, w_r = 80 mm.

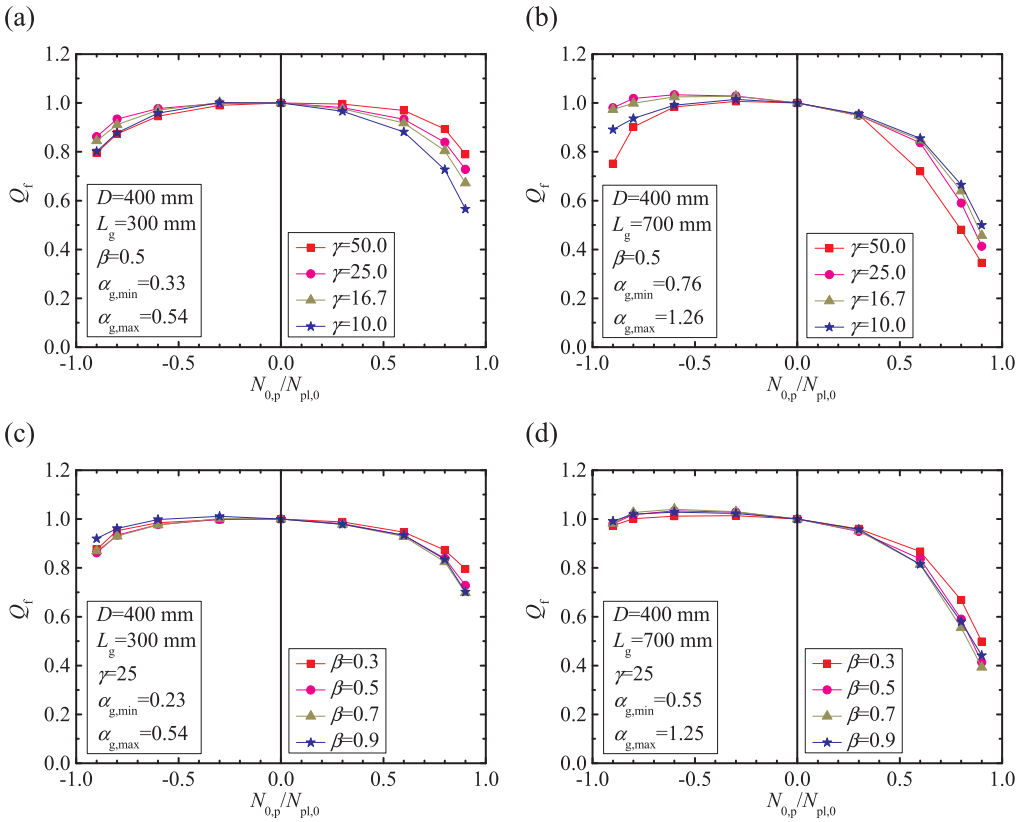

Fig. 12. Chord stress function for joints under axial loads (Scheme 3). (a) L_g = 300 mm, β = 0.5; (b) L_g = 700 mm, β = 0.5; (c) L_g = 300 mm, γ = 25; (d) L_g = 700 mm, γ = 25.

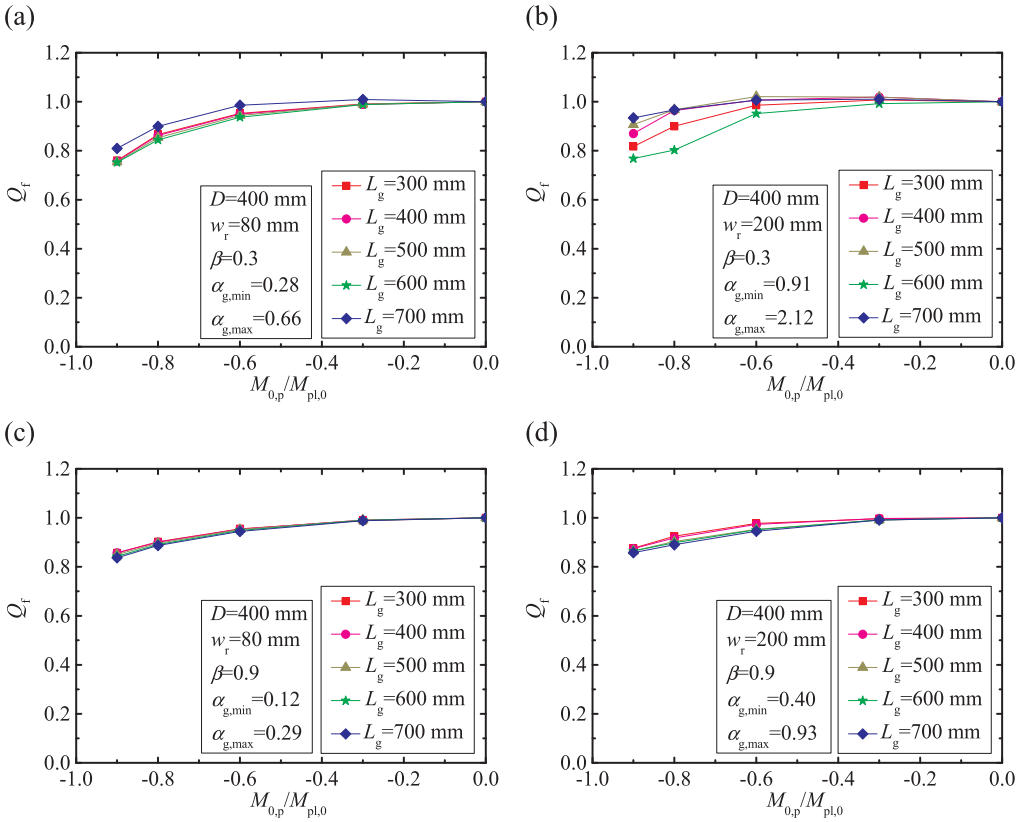

Fig. 13. Chord stress function for joints under in-plane bending moment (Scheme 1). (a) β = 0.3, w_r = 80 mm; (b) β = 0.3, w_r = 200 mm; (c) β = 0.9, w_r = 80 mm; (d) β = 0.9, w_r = 200 mm.

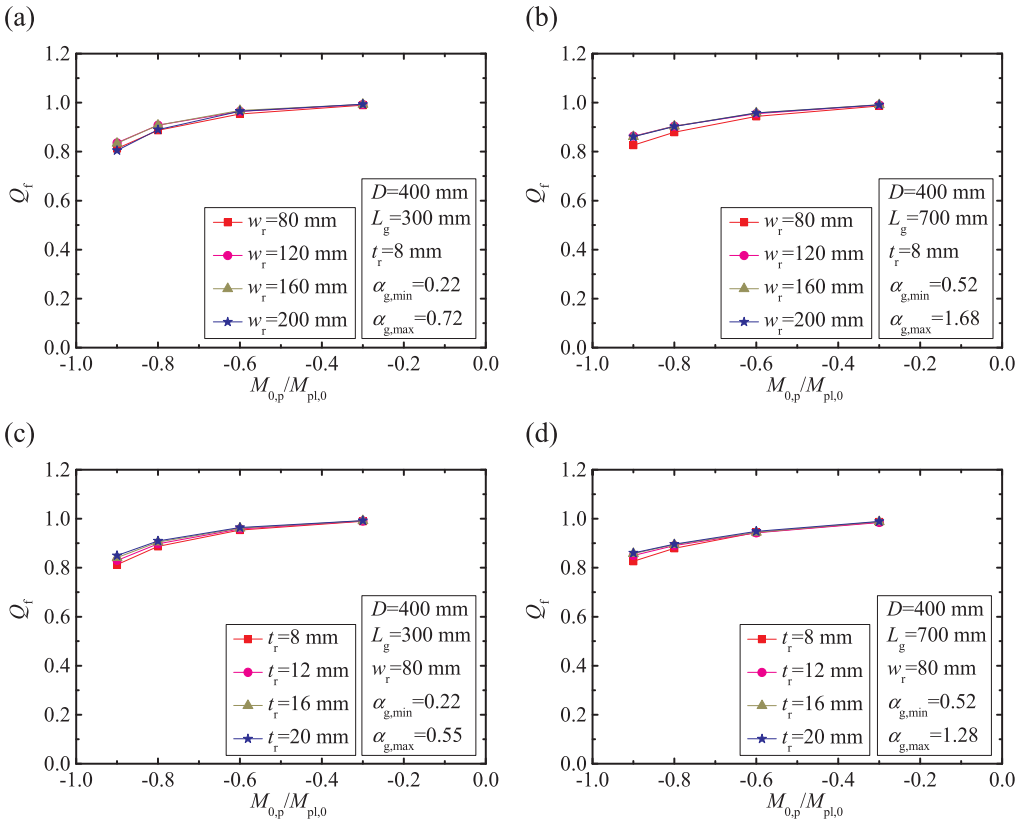

Fig. 14. Chord stress function for joints under in-plane bending moment (Scheme 2). (a) L_g = 300 mm, t_r = 8 mm; (b) L_g = 700 mm, t_r = 8 mm; (c) L_g = 300 mm, w_r = 80 mm; (d) L_g = 700 mm, w_r = 80 mm.

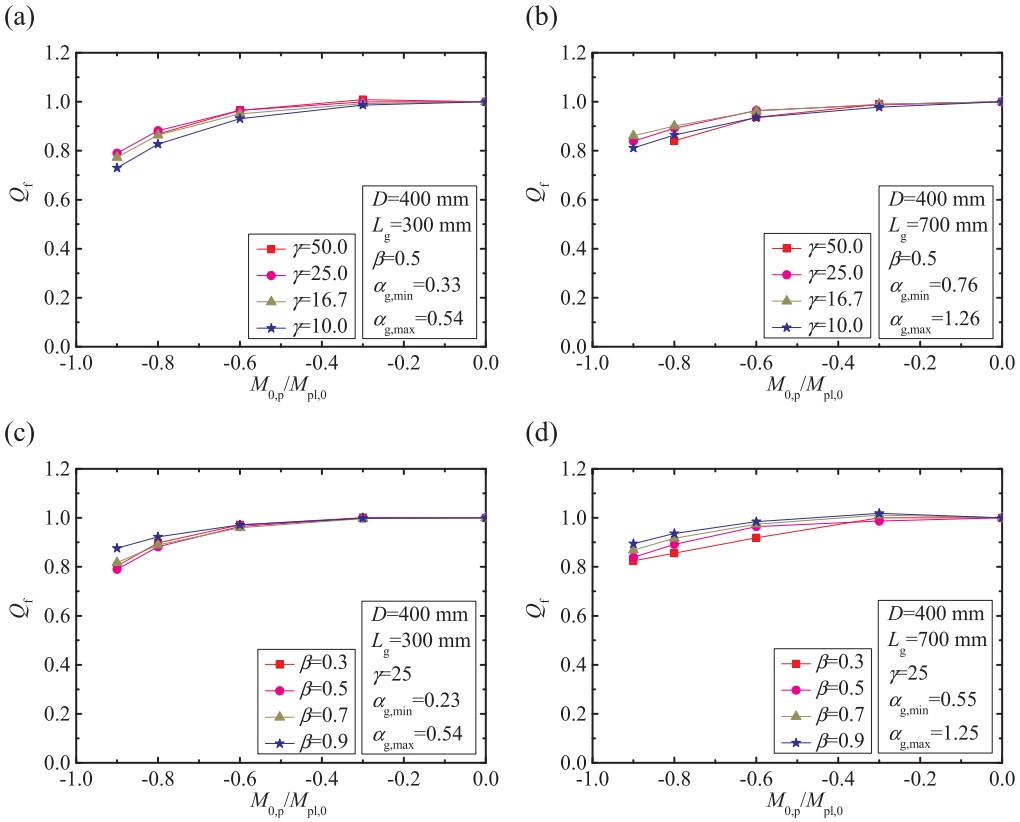

Fig. 15. Chord stress function for joints under in-plane bending moment (Scheme 3). (a) L_g = 300 mm, β = 0.5; (b) L_g = 700 mm, β = 0.5; (c) L_g = 300 mm, γ = 25; (d) L_g = 700 mm, γ = 25.

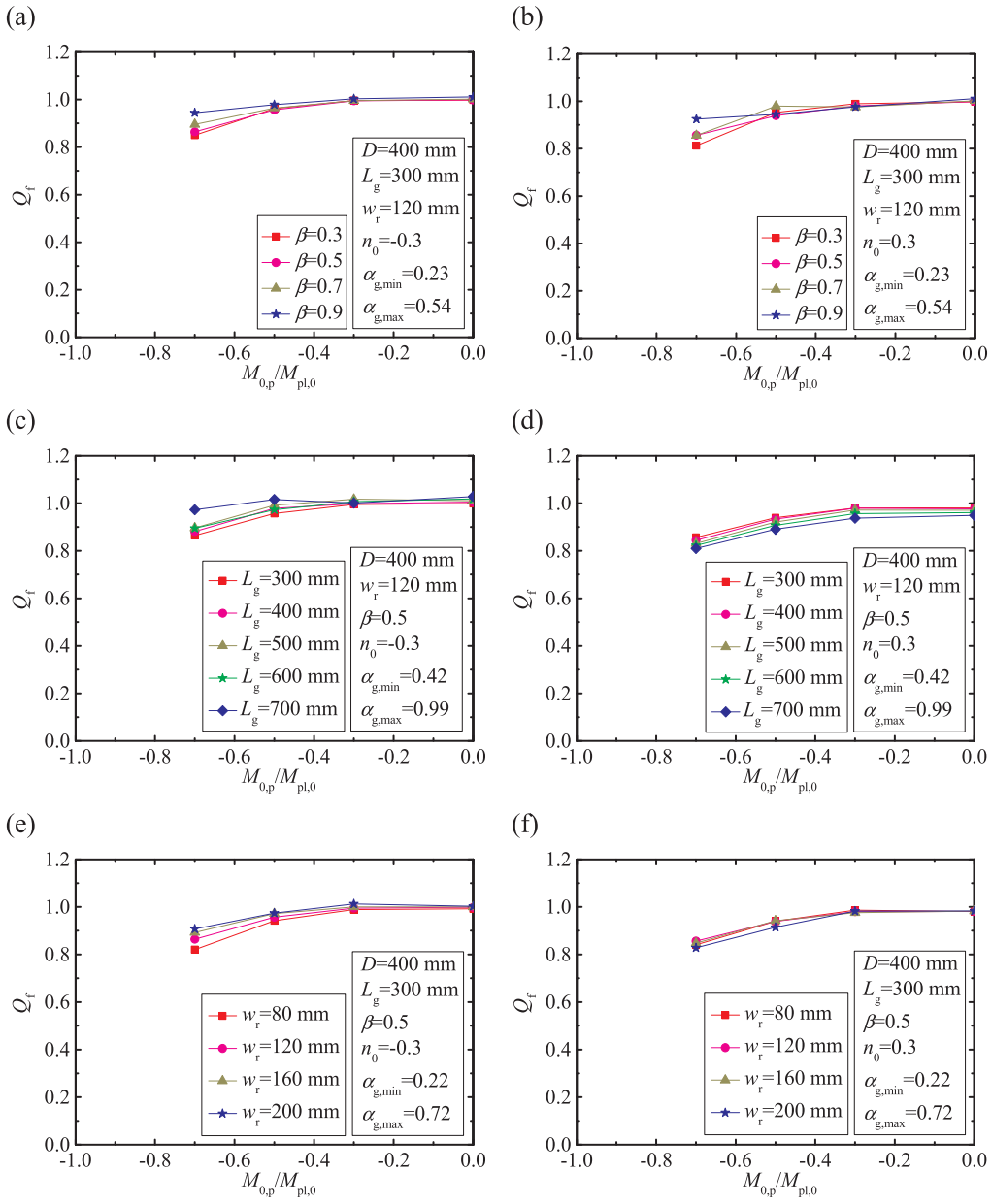

Fig. 16. Chord stress function against $M_{0,p}/M_{pl,0}$ for joints under combination of axial force and in-plane bending moment (Scheme 1). Effect of (a) β with $n_0 = -0.3$; (b) β with $n_0 = 0.3$; (c) L_g with $n_0 = -0.3$; (d) L_g with $n_0 = 0.3$; (e) w_r with $n_0 = -0.3$; (f) w_r with $n_0 = 0.3$.

(20) are close to the results obtained via the formulas recommended by CIDECT, whereas the results of Q_f attained via Eq. (18) are close to that via API formulas. If one uses the chord stress function specified for unstiffened X-joint in designing a stiffened X-joint, the above findings imply that these formulae are rather conservative if the chord is under compression. However, these formulae cannot effectively account for the reduction of bearing capacity caused by the presence of chord tension. Especially, the equations recommended by AISC, which neglect the effect of reduction due to chord pre-tension, are not consistent with the updated research, and are not applicable for the stiffened X-joints with chord under tension.

In order to gain a more comprehensive understanding of the differences between the proposed formulae and the formulae recommended by specifications, the values of chord stress functions of all stiffened X-joints in Scheme 1 are calculated and shown in Fig. 22. The results are presented in terms of the ratio of chord stress function in specifications to proposed one, namely $Q_{f,X}/Q_{fd}$, where $Q_{f,X}$ is the chord stress function in which subscript 'X' stands for 'CIDECT', 'AISC' or 'API'. As mentioned above, if the chord stress function for the unstiffened joints is used for the stiffened X-joints, in case of $\mathrm{sgn}(n_0) < 0$, the values via the proposed formula are generally greater, and the deviation of $Q_{f,X}/Q_{fd}$ is small. Moreover, for $\mathrm{sgn}(n_0) > 0$, the results of the proposed formula appear to be much smaller, and the deviation is remarkable. The above facts are in consistent with the aforementioned findings achieved via numerical and theoretical analysis.

6. Conclusions

Effects of chord pre-loads on ultimate bearing capacity of a newly developed stiffened X-joint are investigated. An elaborate FE model is established to examine the mechanic performance of the stiffened X-joints subjected to both chord and brace loadings. The FE model is validated by test results. Non-proportional loading is taken for numerical study, since the preliminary study on load path indicates that the effect of loading path on the ultimate bearing capacity is negligible. Conclusions can be drawn as follows:

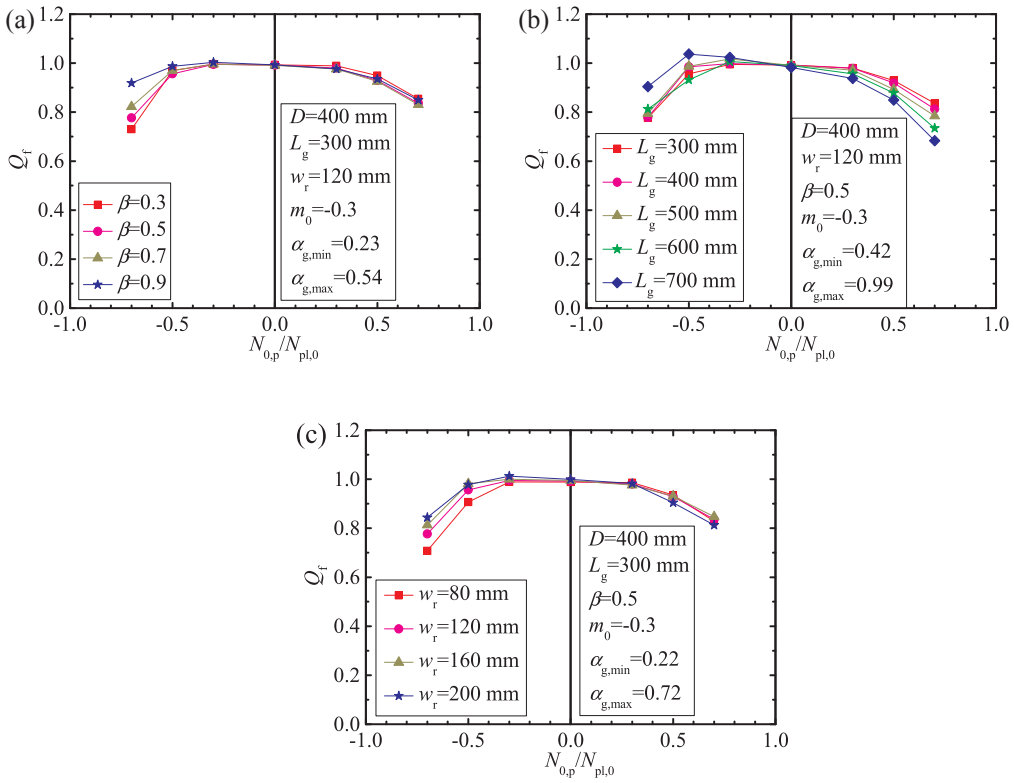

Fig. 17. Chord stress function against $N_{0,p}/N_{pl,0}$ for joints under combination of axial force and in-plane bending moment (Scheme 1). Effect of (a) β with $m_0 = -0.3$; (b) L_g with $m_0 = -0.3$; (c) w_r with $m_0 = -0.3$.

(1) For unstiffened X-joints, the effect of chord tension on bearing capacity is conventionally considered much smaller than that of chord compression. However, the study indicates that a remarkable reduction in bearing capacity can occur in the stiffened X-joints when the chords are under tension. Furthermore, in case of chord compression, the bearing capacity of stiffened X-joint is slightly affected by the axial chord load, and sometimes even improved. The different chord stress effects found in the stiffened and unstiffened X-joints are attributed to the presence of gusset plates and ring plates. Compared to unstiffened X-joint, stiffened X-Joint has a much smaller effect of axial chord pre-load on resistance of chord wall, and a relatively greater effect on resistance of chord rings. Since the resistance of chord rings usually predominates, the effect of axial chord pre-load on overall bearing capacity of stiffened X-joint is similar to that on strength of chord rings.

(2) For stiffened X-joints subjected to in-plane bending moments, the

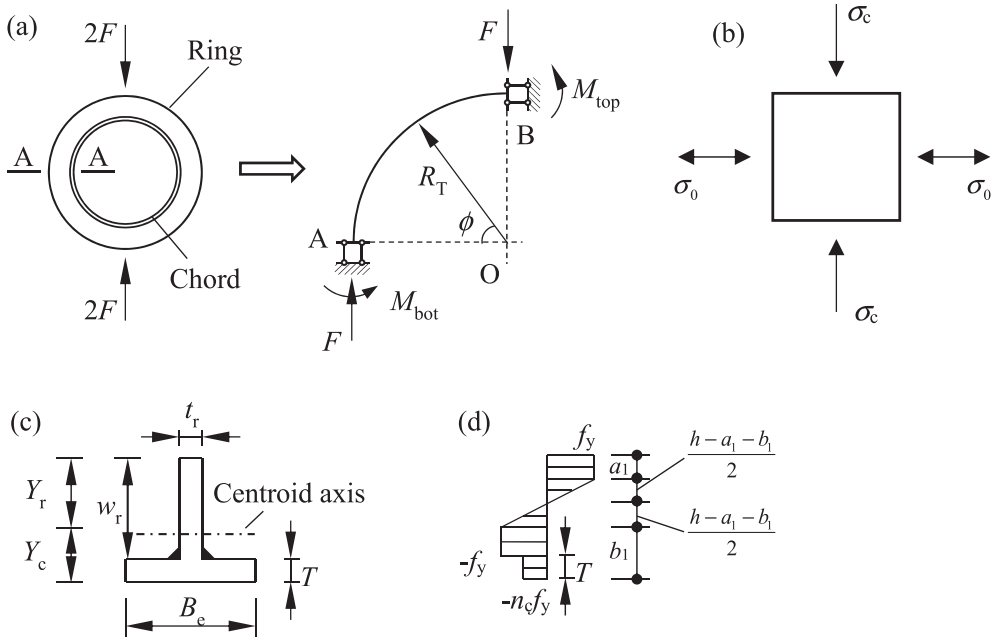

Fig. 18. Simplified model schematic diagram. (a) Simplified curved beam for ring model; (b) chord wall element under in-plane stress state; (c) geometric parameters for T-shape section; (d) stress distribution on T-shape section.

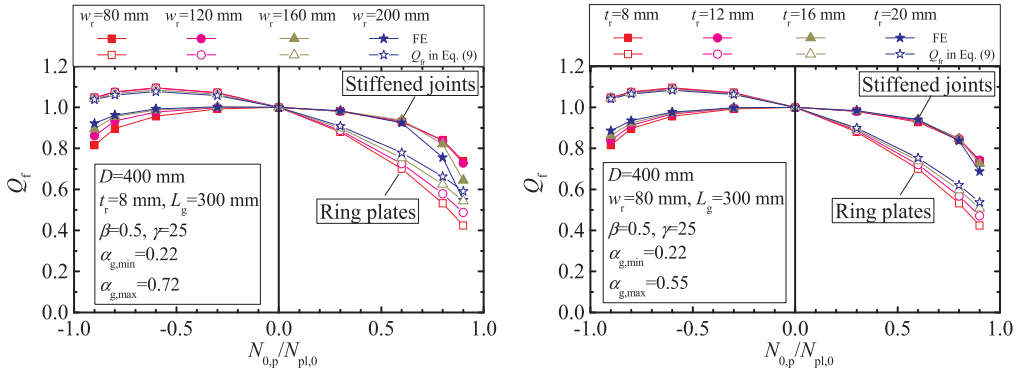

Fig. 19. Effect of axial chord loads on chord stress function of ring plates and stiffened joints with (a) t_r = 8 mm; or (b) w_r = 80 mm.

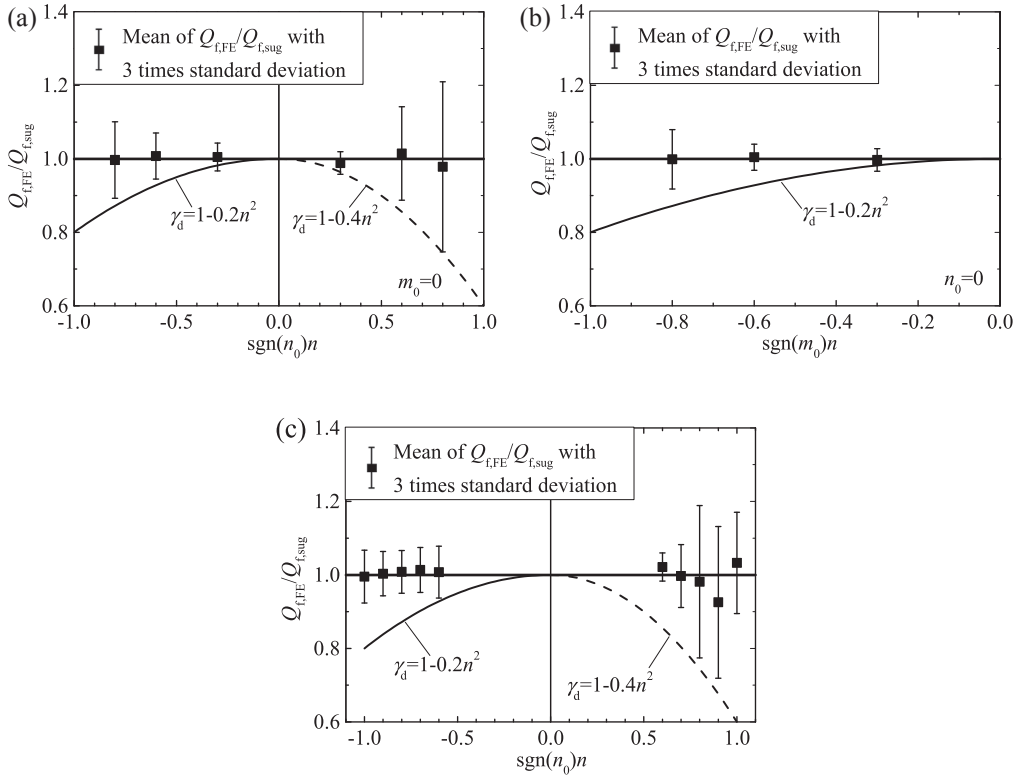

Fig. 20. Curves of lower-bound multiplier and dispersion of $Q_{f,FE}/Q_{f,sug}$ with varying n_0 for joints with chord preloads of (a) axial force; (b) bending moment; or (c) combination of axial force and bending moment.

effect of chord stress can be regarded as a superposition of the effects of axial tension and axial compression. The value of chord stress function decreases as the bending moment increases, and the amount of the decrease is greater than that in case of chord tension. This is related to the fact that half of the chord section is under compression and half is under tension, when the chord is merely subjected to in-plane bending moment.

(3) In case of chord subjected to combination of axial force and in-plane bending moment, the effect of axial compression on bearing capacity of stiffened X-joint is similar to that of axial tension, due to the presence of the in-plane bending moment. That is, a significant reduction in bearing capacity can be observed in both cases of chord compression and chord tension, which differs from the observation in the stiffened X-joints with the chord merely subjected to axial load.

(4) The theoretical analysis shows that the chord tension can reduce the resistance of the chord rings, which is the main reason for the reduction of overall bearing capacity of the whole joint. This conclusion was further supported by the numerical analysis. Since the strength of chord ring is the dominant factor in the total bearing capacity, the formulas have been derived for calculating the strength of chord rings with chord stress in presence, based on which an empirical formula can be deduced to evaluate the chord stress function of stiffened X-joint. This is practically more feasible than pure theoretical approaches.

(5) Taking into consideration different chord pre-loads, an empirical formula of chord stress function is proposed. In order to balance accuracy and convenience, different values of the coefficients in formula is suggested for different cases of chord pre-loads. Overall, the formula based on substantial results of FE analyses has a good accuracy, especially in case of chord compression. To compensate for the increasing dispersion at large n, a lower-bound multiplier is introduced to ensure the design being on a slightly conservative side.

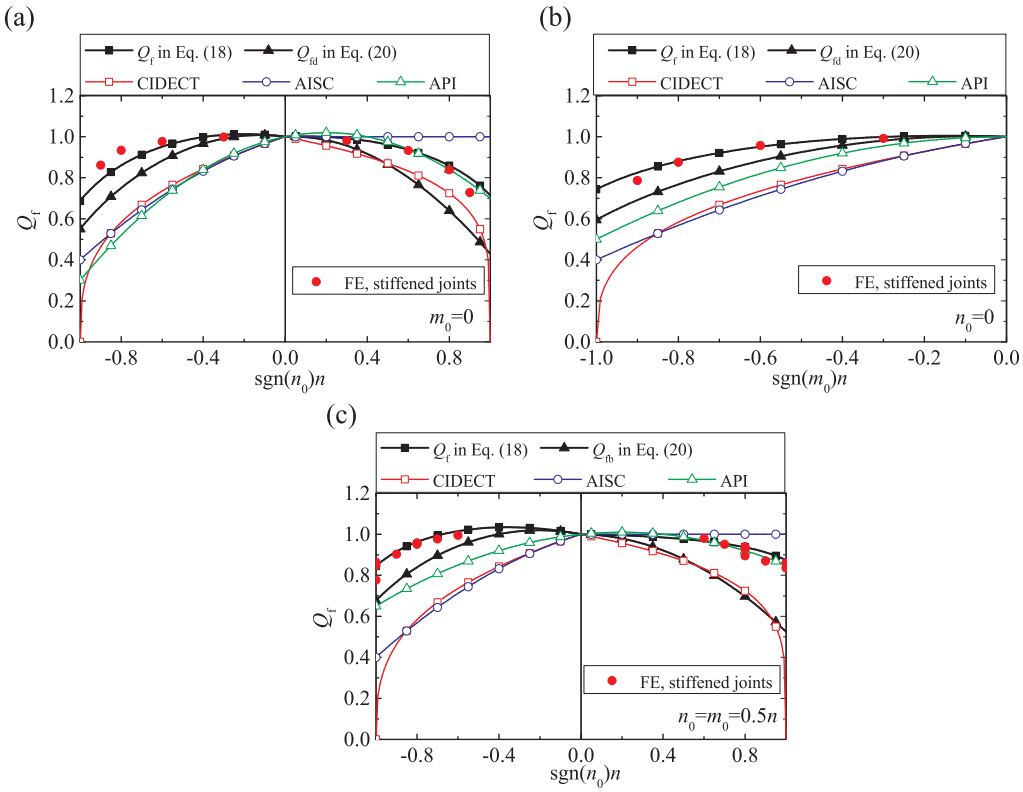

Fig. 21. Comparison between proposed equations and reported chord stress function for joints with (a) axial load; (b) bending moment; or (c) combination of axial load and bending moment.

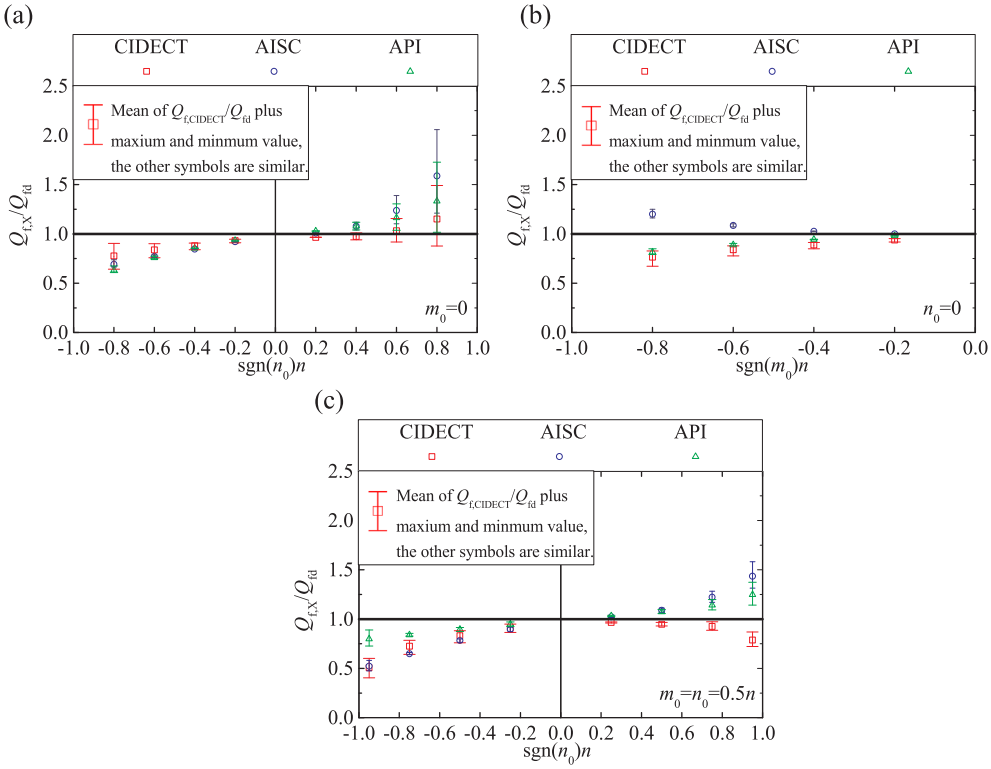

Fig. 22. Comparison between proposed equations and reported chord stress function for joints (Scheme 1) with (a) axial load; (b) bending moment; or (c) combination of axial load and bending moment.

Acknowledgments

The authors would like to acknowledge the financial support of State Grid Science and Technology Project (5211JH13527C, SGTYHT/15-JS-193) and National Natural Science Foundation of China (51878607, 51838012).

Appendix A. Supplementary material

Supplementary data to this article can be found online at https://doi.org/10.1016/j.engstruct.2019.05.076.

References

[1] Chen Y, Hu Z, Guo Y, Wang J, Dan H, Liu Q, et al. Ultimate bearing capacity of CHS X-joints stiffened with external ring stiffeners and gusset plates subjected to brace compression. Eng Struct 2019;181:76–88.
[2] Togo T. Experimental study on mechanical behavior of tubular joints. . Osaka, Japan PhD Thesis, Osaka Univ. 1967. (in Japanese).
[3] Boone TJ, Yura JA, Hoadley PW. Ultimate strength of tubular joints: chord stress effects. Offshore Technol Conf 1984:437–46.
[4] Weinstein RM, Yura JA. The effect of chord stresses on the static strength of DT tubular connections. Offshore Technol Conf 1986:447–51.
[5] Ha CC, Pecknold DA, Mohr WC. FE modeling of DT tubular joints with chord stress. 17th Int. Conf. Offshore Mech. Arct. Eng. 1998. p. 1–10.
[6] Pecknold DA, Ha CC, Mohr WC. Chord stress effects on ultimate strength of DT tubular joints. 17th Int. Conf. Offshore Mech. Arct. Eng. 1998. p. 1–8.
[7] Pecknold DA, Ha CC, Mohr WC. Ultimate strength of DT tubular joints with chord preloads. Proc. 19th Int. Conf. Offshore Mech. Arct. Eng. 2000. p. 425–36.
[8] Kang CT, Moffat DG, Mistry J. Strength of DT tubular joints with brace and chord compression. J Struct Eng 1998;124:775–83.
[9] Kang CT, Moffat DG, Mistry J. Ultimate strength of a double-tee tubular joint subjected to combined chord compression and brace out-of-plane bending. J Strain Anal Eng Des 1998;33:385–94.
[10] Van der Vegte GJ, Makino Y. The effect of chord stresses on the statics strength of CHS X-joints. Mem Fac Eng Kumamoto Univ 2001;46:1–24.
[11] Van der Vegte GJ, Wardenier J, Makino Y. Effect of chord load on ultimate strength of CHS X-joints. Int J Offshore Polar Eng 2007;17:301–8.
[12] Choo YS, Qian XD, Liew JYR, Wardenier J. Static strength of thick-walled CHS X-joints – part II. Effect of chord stresses. J Constr Steel Res 2003;59:1229–50.
[13] Qian XD, Choo YS, Van der Vegte GJ, Wardenier J. Evaluation of the new IIW CHS strength formulae for thick-walled joints. Proc. 12th Int Symp. Tubul. Struct. Shanghai. Taylor Fr. London. 2008. p. 271–80.
[14] Van der Vegte GJ, Wardenier J, Zhao XL, Packer JA. Evaluation of new CHS strength formulae to design strengths. Proc. 12th Int. Symp. Tubul. Struct. Shanghai, China. Taylor Fr. Gr. 2008. p. 313–22.
[15] Pecknold D, Marshall P, Bucknell J. New API RP2A tubular joint strength design provisions. J Energy Resour Technol 2007;129:177–89.
[16] Dier AF, Lalani M. New code formulations for tubular joint static strength. A A Balkema Publ Tubul Struct VIII(USA). 1998. p. 107–16.
[17] Young WC, Budynas RG. Roark's formulas for stress and strain. Seventh Ed McGraw-Hill 2002.
[18] Lee MMK, Llewelyn-Parry A. A theoretical model for predicting strength of ring-stiffened tubular T-joints in offshore structures. Proc Inst Civ Eng - Struct Build 1999;134:19–31.
[19] Wardenier J, Kurobane Y, Packer JA, Van der Vegte GJ, Zhao XL. Design guide for circular hollow section (CHS) joints under predominantly static loading. 2nd Editio. CIDECT. 2008.
[20] Welding of International Institute. Static design procedure for welded hollow section joints—Recommendations. IIW Doc. XV-1402-12; 2012.
[21] International Organization for Standardization. Static design procedure for welded hollow-section joints - Recommendations. 2013.
[22] Packer J, Sherman D, Hollow Lecce M. Structural Section Connections. American Institute of Steel Construction. 2010.
[23] American Petroleum Institute. Planning, Designing, and Constructing Fixed Offshore Platforms - Working Stress Design, RP 2A-WSD. 22nd editi. 2014.
[24] Wardenier J. Hollow Section Joints. Technische Universiteit of Delft. 1982.